### Title

A single double-strand break system reveals repair dynamics and mechanisms in heterochromatin and euchromatin




### Journal

Genes & Development, 30(14)

### ISSN

0890-9369



### Authors

Janssen, Aniek
Breuer, Gregory A
Brinkman, Eva K
et al.



### Publication Date

2016-07-15

### DOI

10.1101/gad.283028.116

Peer reviewed

# A single double strand break system reveals repair dynamics and mechanisms in heterochromatin and euchromatin

Aniek Janssen[1], Gregory A. Breuer[2], Eva K. Brinkman[3], Annelot I. van der Meulen[1], Sean V. Borden[1], Bas van Steensel[3], Ranjit S. Bindra[2], Jeannine R. LaRocque[4,6] and Gary H. Karpen[1,5,6]

[1] Biological Systems and Engineering Division, Lawrence Berkeley National Laboratory, Berkeley, California, USA

[2] Departments of Therapeutic Radiology and Experimental Pathology, Yale School of Medicine, New Haven, Connecticut, USA

[3] Division of Gene Regulation, Netherlands Cancer Institute, Amsterdam, the Netherlands

[4] Department of Human Science, School of Nursing & Health Studies, Georgetown University Medical Center, Washington DC, USA

[5] Department of Molecular and Cell Biology, UC Berkeley, Berkeley, California, USA

[6] Correspondence should be addressed to ghkarpen@lbl.gov or Jan.LaRocque@georgetown.edu

Running title: Double strand break repair in Drosophila heterochromatin

Keywords: heterochromatin, recombination repair, cell cycle, homolog, NHEJ, Drosophila

**Abstract**

Repair of DNA double-strand breaks (DSBs) must be properly orchestrated in diverse chromatin regions to maintain genome stability. The choice between two main DSB repair pathways, non-homologous end joining (NHEJ) and homologous recombination (HR), is regulated by the cell cycle as well as chromatin context. Pericentromeric heterochromatin forms a distinct nuclear domain that is enriched for repetitive DNA sequences that pose significant challenges for genome stability. Heterochromatic DSBs display specialized temporal and spatial dynamics that differ from euchromatic DSBs. Although HR is thought to be the main pathway used to repair heterochromatic DSBs, direct tests of this hypothesis are lacking. Here, we developed an *in vivo* single DSB system for both heterochromatic and euchromatic loci in *Drosophila melanogaster*. Live imaging of single DSBs in larval imaginal discs recapitulates the spatio-temporal dynamics observed for IR-induced breaks in cell culture. Importantly, live imaging and sequence analysis of repair products reveal that DSBs in eu- and hetero-chromatin are repaired with similar kinetics, employ both NHEJ and HR, and can use homologous chromosomes as an HR template. This direct analysis reveals important insights into heterochromatin DSB repair in animal tissues, and provides a foundation for further explorations of repair mechanisms in different chromatin domains.

**Introduction**

The eukaryotic nucleus contains distinct chromatin domains called heterochromatin and euchromatin (Heitz 1928). Constitutive heterochromatin is

enriched for repetitive DNAs and contains few protein-coding genes. In contrast, euchromatin is generally associated with more open chromatin regions and contains many actively transcribed genes. Heterochromatin is predominantly concentrated at pericentromeric and telomeric regions, and disruption of heterochromatin impairs chromosome segregation, replication timing, transposon silencing and gene expression (Weiler and Wakimoto 1995; Peters et al. 2001; Peng and Karpen 2009; Rangan et al. 2011). Epigenetically, heterochromatin is enriched for di- and tri-methylation of histone H3 lysine 9 (H3K9me2/3) and its binding partner Heterochromatin Protein 1 (HP1) (Eissenberg and Elgin 2000).

Changes in H3K9 methylation levels and distributions are seen in aging (Chen et al. 2014) and cancer (Sulli et al. 2012; Ellinger et al. 2014). Moreover, H3K9me2-rich genomic regions are highly correlated with increased mutation load in a variety of cancer types (Schuster-Bockler and Lehner 2012), suggesting that heterochromatin regions are more susceptible to DNA damage and improper repair. Thus, determining how DNA repair in heterochromatic DNA is regulated will elucidate how chromatin states impact genome stability, and how misregulation contributes to disease progression.

One of the most deleterious DNA lesions is a double-strand break (DSB), since improper DSB repair can lead to formation of aberrant chromosomes (e.g., translocations and insertions) that contribute to cancer and developmental diseases (Janssen and Medema 2013). DSBs can occur during endogenous processes, such as replication fork collapse upon encountering an unrepaired DNA lesion, or by exogenous mutagens such as irradiation (IR) (Ciccia and Elledge

2010). The two main DSB repair pathways are homologous recombination (HR), in which a homologous template is used to accurately repair the DSB, and the more error-prone non-homologous end joining (NHEJ) pathway, in which two broken DNA ends are ligated together, often resulting in modifications of bases at the break site. HR is mainly limited to the S and G2 cell cycle phases, when a sister chromatid is present and can be used as a recombination template. In contrast, NHEJ can be used at any stage of the cell cycle (Ciccia and Elledge 2010).

The importance of specific chromatin modifications and remodelers in DSB repair and pathway choice has become increasingly clear over the past decade (Price and D'Andrea 2013). For example, H3K36 trimethylation at actively transcribed regions is associated with a preference for HR repair (Aymard et al. 2014), and specific chromatin environments can predispose a genome to translocations (Burman et al. 2015) or repair by the error prone alternative NHEJ (Lemaitre et al. 2014).

DSBs in constitutive heterochromatin are considered especially dangerous, due to the presence of many homologous repetitive sequences on different chromosomes. HR repair of damaged repeats can result in aberrant recombination products that are harmful for cells and organisms (Chiolo et al. 2011; Ryu et al. 2015). However, studies in mammalian and *Drosophila melanogaster* cultured cells do suggest that HR is the main repair pathway utilized by heterochromatic DSBs (Goodarzi et al. 2008; Chiolo et al. 2011; Goodarzi and Jeggo 2012). Heterochromatic DSBs display specific temporal and spatial responses that differ significantly from euchromatic DSBs. In Drosophila and mammalian cell culture,

heterochromatic DSBs induced by IR relocalize to outside the heterochromatin domain (Chiolo et al. 2011; Jakob et al. 2011). 5' to 3' end-resection, phosphorylation of H2Av by ATM/ATR kinases (γH2Av, analogous to γH2AX in mammals (Rogakou et al. 1999)) and recruitment of proteins that regulate early events in HR repair (e.g. ATRIP and TopBP1) occur at heterochromatic DSBs inside the domain, within minutes after IR. However, proteins involved in late HR events (e.g. BRCA2, Rad51) are recruited to DSBs only after they relocalize (Chiolo et al. 2011). We hypothesized that these spatial and temporal dynamics help prevent aberrant recombination events between repetitive regions on non-homologous chromosomes, and promote 'safe' recombination between sister chromatids or homologs. However, it is currently unclear if heterochromatin-specific DSB relocalization to the nuclear periphery depends on induction of many breaks at the same time (using IR), or if a single break induces the same dynamic behaviors.

A key role for HR also was demonstrated by genetic analyses. Depletion of HR proteins in Drosophila cells, but not NHEJ proteins, resulted in retention of IR-induced repair foci inside the heterochromatin domain (Chiolo et al. 2011). However, direct determination of all DSB repair pathways utilized, as well as information about the templates used for HR, requires sequence analysis of repair products (Nagel et al. 2014; Soong et al. 2015), which is difficult for repetitive DNA. Thus, other pathways, such as NHEJ or single-strand annealing (SSA), could also play an important role in repairing heterochromatic DSBs. In fact, utilization of NHEJ would eliminate some aberrant repair events that result from HR between repetitive regions. In SSA, extensive end resection results in annealing of

complementary repetitive sequences, which could be of particular importance in repeat-rich heterochromatin. Determining if the NHEJ and SSA pathways impact heterochromatin DSB repair is important to understand the mechanisms that maintain the stability of repeated DNAs.

To address these questions, we developed a *Drosophila melanogaster* single DSB system to analyze repair in both constitutive heterochromatic and euchromatic sites. Drosophila is an attractive system to study DSB repair in the context of a living organism with well-characterized chromatin environments (Kharchenko et al. 2011), effective tools for analyzing repair processes (Rong and Golic 2003; Preston et al. 2006; Do et al. 2014), and conservation of heterochromatin regulation and protein complexes with mammals (Fodor et al. 2010; Hoskins et al. 2015).

Here we show that single heterochromatic DSBs relocalize from the heterochromatin domain in living tissues and show similar repair kinetics as euchromatic DSBs. Most importantly, in contrast to earlier findings, genetic as well as sequence analyses revealed that NHEJ, SSA and HR pathways are used to repair heterochromatic DSBs, at frequencies similar to euchromatic DSBs. Finally, we developed an *in vivo* homolog-tracking system that demonstrates that both eu– and hetero-chromatic DSBs can utilize homologs as a template for HR repair. These findings advance our knowledge of the components and mechanisms that repair heterochromatic DSBs and ensure genome stability.

## Results

### Development of a single DSB system for hetero- and eu-chromatic loci

We developed a single DSB system to cytologically compare DNA damage repair in euchromatic and constitutive heterochromatic loci in animal tissues, and to determine pathway utilization by DNA sequence analysis of DSB repair products. Specifically, we used the MiMIC system (Venken et al. 2011) to integrate the DR-*white* DSB reporter (Do et al. 2014) into six pericentromeric heterochromatic and three euchromatic loci (Fig. 1A, B).

The DR-*white* reporter has one upstream non-functional *white* gene (*white* expression results in red-eye color) containing an I-SceI recognition sequence, a red fluorescent marker (3xp3-dsRed) and a downstream truncated, non-functional *white* gene (*iwhite*) (Fig. 1A). DsRed and *white* are driven by the eye tissue-specific promoters 3xP3 and glass multiple reporter (GMR), respectively. The upstream *white* gene contains a premature stop codon present in the I-SceI recognition sequence (Do et al. 2014). Expression of the rare cutting endonuclease I-SceI, used extensively in studies of DSB repair (Jasin 1996), induces a single DSB at the I-SceI cut site. Repair of this single DSB by HR, NHEJ, and SSA occurs in the germline as well as somatic cells. Relative contributions of each of these pathways can be quantitated by determining the phenotypes of the progeny (pre-meiotic male germline repair events), or by PCR and sequence analysis (somatic and germline repair events) (Fig. 1A).

We confirmed integration of all DR-*white* constructs in the targeted genomic loci (Fig. 1B) using PCR. In addition, we performed Chromatin

Immunoprecipitation followed by quantitative PCR (ChIP-qPCR) using an antibody that specifically recognizes H3K9me3, the key heterochromatin-enriched histone modification (Fig. 1C). As expected, the three euchromatic DR-*white* insertions were not enriched for H3K9me3, whereas the six heterochromatic DR-*white* insertions showed an 8 to 90-fold enrichment of H3K9me3 at the I-SceI cut site compared to input (Fig. 1C). H3K36me3 has been linked to DSB repair pathway choice (Aymard et al. 2014) and introduction of DR-*white* insertions could potentially affect this transcription-associated mark. However, the expression of dsRed is under the control of an eye tissue-specific driver, and we observed strong silencing of dsRed in all heterochromatic DR-*white* insertions (data not shown). In addition, ChIP-qPCR analysis showed no change in H3K36me3 enrichment at DR-*white* insertions in comparison to Modencode ChIP-seq data from wild type larval tissue (Fig. S1A). Finally, Fluorescence In Situ Hybridization (FISH) on fixed larval imaginal discs with probes recognizing DR-*white* and the AACAC repeat, present in chromosome 2R heterochromatin, cytologically validated the DR-*white* integrations in heterochromatin. Consistent with the observed H3K9me3 patterns, heterochromatic DR-*white* integrations were spatially close (500nm) to the AACAC repeat, whereas the euchromatic DR-*white* insertion on chromosome 2 was on average 1200nm separated from the AACAC repeat (Fig. 1D).

In order to temporally control DSB formation, we utilized two different inducible I-SceI expression systems (Fig. 1E). Fusing I-SceI to an ecDHFR degradation domain (ecDHFR-I-SceI) allows I-SceI protein stabilization after addition of the ligand Trimethoprim (Cho et al. 2013). Hsp70.I-SceI is a heat-shock

inducible system with hsp70 promoter-dependent I-SceI expression (Rong and Golic 2003) (Fig. 1E). Three hours after incubating larval imaginal discs containing both ecDHFR-I-SceI and DR-*white* in medium containing Trimethoprim, 4-8% of cells showed one γH2Av focus compared to 1-3% in controls (DMSO only) (Fig. 1F), indicating that single DSBs can be temporally induced using the ligand-dependent system. Expression of ecDHFR-I-SceI after feeding larvae Trimethoprim did not produce visible cell cycle defects or reduce organismal or cell viability, ruling out specific cell cycle or lethality-associated effects of the ecDHR-I-SceI system (Fig. S1B-D). The hsp70.I-SceI transgene was more efficient at inducing single DSBs, since 13-20% of imaginal disc cells contained a single γH2Av focus six hours after heat shock, compared to 4% in control tissue (no heat shock) (Fig. S1E). We conclude that both systems temporally induce single breaks at DR-*white* loci. In addition, after induction there were no consistent differences in γH2Av foci numbers between euchromatic and heterochromatic loci (Fig. 1F, S1E), ruling out the possibility that heterochromatin regions are less accessible to cleavage by I-SceI.

**Live imaging reveals dynamic movement of single DNA damage foci in heterochromatin.**

We previously discovered that irradiation (IR)-induced DNA damage foci in heterochromatin move to the periphery of the domain in Drosophila cultured cells (Chiolo et al. 2011). To determine if similar movements occur after single DSB induction *in vivo*, we generated DR-*white* fly lines that express ecDHFR-I-SceI and

red fluorescent protein (RFP)-tagged HP1a (marks the heterochromatin domain). To visualize DSBs, these flies also express mu-2 tagged with enhanced yellow fluorescent protein (eYFP); mu2, the Drosophila ortholog of mammalian MDC1, binds to γH2Av and is recruited to DSB sites early in repair (Stucki et al. 2005; Dronamraju and Mason 2009)) (Fig. 2A).

We tracked the nuclear localization of eYFP-mu2 focus appearance and disappearance with respect to the RFP-HP1a heterochromatin domain (Fig. 2A). As expected, the majority (~80%) of mu2 foci in cells containing euchromatic DR-*white* insertions first appear outside of the HP1a domain. In contrast, ~70% of foci in cells containing heterochromatic insertions first appear inside or at the periphery of the HP1a domain (Fig. 2A). 10-15% of mu2 foci associated with DSBs at heterochromatic DR-*white* insertions arose inside the HP1a domain and moved to the domain periphery within one time frame (10 minutes), where they were subsequently resolved, i.e. disappeared (Fig. 2A, dark blue bars). 30-50% of mu2 foci in cells containing heterochromatic DR-*white* insertions appeared at the periphery and stayed there until the mu2 focus resolved (Fig. 2A, red bars). This behavior likely reflects our inability to capture initial mu2 focus localization inside the HP1a domain, due to low time resolution (one image every 10 minutes). Alternatively, some of the uncut DR-*white* insertions could reside at the HP1a domain periphery, making it difficult to see the spatial dynamics observed for foci originating within the HP1a domain. Regardless, we conclude that the temporal and spatial relocation dynamics for I-SceI-induced single breaks in live tissues recapitulated our previous observations for IR-induced foci in cultured Drosophila

cells (Chiolo et al. 2011). Interestingly, we also observed a small subset of foci (5-10%) that first appeared in the HP1a domain and were resolved without peripheral movement. This suggests that a small subset of heterochromatic DSBs do not move to the periphery, and could complete repair within the heterochromatin domain.

In addition to data on the spatial movement of mu2 foci, live imaging also allowed direct assessment of the kinetics of mu2 focus appearance (onset of DSB repair) and disappearance (resolution of repair foci; this is not an absolute measure of the repair timing, due to the possible persistence of γH2Av and mu2 after repair is finished (Mah et al. 2010)). Studies using IR in mammalian cells suggested that heterochromatic DSBs display slower repair rates compared to euchromatic DSBs (Goodarzi et al. 2008; Beucher et al. 2009). However, we found that the average time required to resolve mu2 foci was not significantly different between 3 heterochromatic and 3 euchromatic insertions (Fig. 2B). DSBs in both chromatin regions showed similar kinetics; 50% of mu2 foci disappeared within 60 minutes after appearance, and the time from appearance to disappearance displayed a wide range in the remaining 50% of foci, from ~60 to more than 350 minutes (Fig. 2B). We conclude that although there are site-specific differences in mu2 foci kinetics (compare Fig. 2D – controls with Fig.2E – controls (black lines)), there are no significant differences in the average rate of mu2 focus disappearance at eu- versus hetero-chromatic loci, in contrast to previous findings (Goodarzi et al. 2008).

**Live imaging reveals that disruption of HR or NHEJ pathways delays repair kinetics at both heterochromatic and euchromatic DSBs.**

HR has been reported to be the major pathway responsible for repair of DSBs in heterochromatin (Beucher et al. 2009; Chiolo et al. 2011). We previously found that depletion of DmRad51 (HR protein, Rad51, encoded by *spn-A*) in Drosophila cultured cells, but not depletion of DmKu70 (encoded by *Irbp)* or DmKu80 (encoded by *Ku80*) (NHEJ proteins), resulted in defective relocalization and aberrant accumulation of DNA damage foci within heterochromatin following IR (Chiolo et al. 2011).

To more directly analyze the impact of HR and NHEJ pathways on repair of I-SceI-induced single breaks *in vivo*, we depleted HR proteins (DmRad51 or DmCtIP/*CG5872*, required for initiating 5' to 3' end-resection (You and Bailis 2010)), or the NHEJ protein DmKu70 by RNAi (Fig. 2C-E). Live analysis revealed that knockdown of DmRad51, DmCtIP (Fig. 2D, E left) or DmKu70 (Fig. 2D, E right) resulted in significant delays in mu2 foci resolution for both euchromatic (Fig. 2D) and heterochromatic DSBs (Fig. 2E). For example, we observed that after DSB induction at the heterochromatic site 3het_1, 50% of mu2 foci in controls resolved within 50 minutes, which increased to 150 and 200 minutes upon DmRad51 or DmCtIP knockdown, respectively (Fig. 2E left). We also investigated whether absence of HR or NHEJ repair caused defects in relocalization of single heterochromatic DSBs. Depletion of DmRad51, DmCtIP or DmKu70 did not result in detectable DSB relocalization defects in live analysis (Fig. S2A), although it is possible that more subtle effects were missed due to the limited temporal

resolution of this analysis. DmKu70 or DmRad51 knockdown did not alter cell cycle progression in the absence of single breaks, indicating that the effects on foci kinetics are not due to DmKu70 or DmRad51 RNAi-induced cell cycle delays before break induction (Fig. S2B). In addition, RNAi-mediated depletion of vermillion, a protein involved in Drosophila eye pigmentation, did not result in a significant delay in mu2 foci disappearance, ruling out the possibility that RNAi pathway activation is responsible for the observed changes in mu2 foci kinetics (Fig. S2C). We conclude that, in contrast to previous studies, both HR and NHEJ proteins are required for DSB repair in both chromatin environments.

**Repair product analysis reveals the use of HR, SSA and NHEJ repair pathways in heterochromatin.**

In order to more directly determine which pathways play a role in heterochromatin DSB repair, we leveraged the DR-*white* system to quantitate the frequencies of different DSB repair products in the male germline (Do et al. 2014)(Fig. 1A, 3A). Single DSBs were induced in both pre-meiotic germ cells and somatic cells by exposing DR-*white*/hsp70.I-SceI embryos and larvae to heat shock (Do et al. 2014). To assess the frequencies of repair pathway utilization in the germline, adult males containing DR-*white* and hsp70.I-SceI were crossed with control females: red-eyed DR-*white* progeny indicate an HR repair event in the paternal male germline (Figs. 1A and 3A). As expected, we observed HR repair events for all the DR-*white* insertions, both heterochromatic and euchromatic (Fig. 3A). Despite suppression of *white* gene expression in the heterochromatic DR-w*hite*

insertions (Fig. 3A, compare right with left eye of F0 generation), red-eyed progeny could still be quantified for both eu- and hetero-chromatin. The percentages of red-eyed progeny varied from 10-30% among the different DR-*white* integrations, but overall there were no significant differences in HR frequencies observed for eu- and hetero-chromatic insertions. The number of germline SSA events in heterochromatic DR-*white* insertions were relatively low (6-8%) and were comparable to numbers observed at a euchromatic DR-*white* locus (6%) ((Do et al. 2014), Fig. S3A). We conclude that in the male germline, DSB repair in heterochromatin can occur through HR and, to a lesser extent, SSA.

The contribution of NHEJ in DSB repair cannot be readily determined by assessing eye color of offspring (Fig. 1A). In addition, we wished to obtain a comprehensive overview of repair events in somatic cells, not only the germline. Therefore, we induced breaks in flies containing DR-*white* and I-SceI transgenes and subsequently PCR-amplified and Sanger sequenced the upstream *white* gene from whole larval genomic DNA (Fig. S3B). This allows for the identification of HR and NHEJ repair events (limited to small insertions and deletions) but excludes SSA events. The number of identified repair products, determined using the established TIDE algorithm (Brinkman et al. 2014), varied among integration sites (16%-40%), possibly reflecting different efficiencies of I-SceI cutting (Fig. S3C, D). However, this variability was not directly correlated with DR-*white* insertions in either eu- or hetero-chromatin, and is therefore not simply explained by reduced repair efficiency or reduced accessibility of I-SceI cut sites in heterochromatin. In addition, this result shows that temporal induction of I-SceI expression using either

the ecDHFR or hsp70 system generates a sufficient amount of repair products for further detailed analysis.

Next, we determined the proportion of HR and NHEJ products in somatic cells and identified the exact sequences present in all NHEJ products using Illumina sequencing of DR-*white* PCR products. This revealed that eu- and hetero-chromatic DSBs generate both HR and NHEJ repair products (Fig. 3B, C). Surprisingly, only 14-35% of identified repair products resulted from HR (Fig. 3B). In contrast, 65-86% of identified repair products contained small insertions and deletions (indels), demonstrating that the majority of DSBs are repaired by NHEJ (Chiruvella et al. 2013). Sanger sequencing and TIDE analysis (Fig. S3E) revealed similar levels of HR and NHEJ products at specific DR-*white* integrations when compared to Illumina sequencing (compare Fig. 3B and Fig. S3E).

The majority (99-100%, Fig. 3C) of NHEJ products analyzed contained small, 1-4 basepair deletions, with one-basepair deletion products as the most abundant (Fig. S3F). Further analysis revealed that 1.5-4% of these deletion products contained micro-homologies of 2 to > 4 basepairs (Fig.S3G), suggesting that micro-homology mediated Alt-EJ (MMEJ) could play a minor role in both eu- and hetero-chromatin repair.

Cell cycle differences between animals with different DR-*white* integration sites could potentially affect the repair pathway analysis. However, comparing cell cycle profiles of actively dividing larval wing discs with both hetero- and eu-chromatic DR-*white* insertions (2 each) using the Fly-FUCCI system (Zielke et al.

2014) (Fig. S4A) did not reveal any overt cell cycle differences that could impact results from the sequence analysis.

In order to confirm the role of HR and NHEJ proteins in DSB repair in eu- and hetero-chromatin, we performed RNAi-mediated knock down of DmKu70 (Fig. 4A), DmRad51 (Fig. 4B) or DmCtIP (Fig. 4C) in DR-*white*/I-SceI larvae and analyzed the repair products. DmRad51 or DmCtIP depletion reduced the proportion of TIDE-identifiable HR events (Fig. 4B,C) for euchromatic and heterochromatic DR-*white* integrations, confirming roles for HR in both chromatin compartments. However, knockdown of DmRad51 or DmCtIP also significantly reduced the total amount of repair products in 2 of 3 and 1 of 2 DR-*white* insertions, respectively (Fig. S4B, C). This suggests that in the absence of DmRad51 or DmCtIP, DSBs either remain unrepaired or employ an alternative pathway (e.g. SSA) (Do et al. 2014), which is undetectable in this PCR-sequence analysis.

We also observed that DmKu70 depletion significantly increased the proportion of HR products (Fig. 4A) and decreased the proportion of indels (NHEJ) (Fig. S4D, E). Interestingly, in contrast to depletion of HR proteins, loss of DmKu70 was not accompanied by a significant decrease in the total amount of identified repair products (Fig. S4D, E). This result suggests that eu- and hetero-chromatic DSBs can be repaired by HR in the absence of a functional NHEJ pathway.

Overall, the frequencies of HR and NHEJ repair products, as well as dependency on canonical HR and NHEJ proteins, were similar for both eu- and hetero-chromatic DR-*white* insertions. Thus, we conclude that HR as well as NHEJ are utilized for DSB repair in both euchromatic and heterochromatic regions.

Finally, DSBs in both chromatin domains can utilize HR when NHEJ is inhibited; however further studies are needed to determine if other repair pathways are utilized upon loss of HR proteins.

**Homologous chromosomes are paired in the presence and absence of DSB induction, but infrequently serve as a template for HR repair.**

HR repair in the DR-*white* reporter system could involve recombination with homologous sequences *in cis* using the downstream *iwhite* sequence, or *in trans* using *white* or *iwhite* on the homolog or sister chromatid. In Drosophila, homologous chromosomes are paired throughout the cell cycle (McKee 2004)(Fig. 5A). The homolog can be used efficiently as a template for HR in Drosophila (Rong and Golic 2003), while its use is more limited in both mammals and yeast (Kadyk and Hartwell 1992; Liang et al. 1998; Johnson and Jasin 2000).

In order to evaluate utilization of the homologous chromosome as a template for HR repair in both eu- and hetero-chromatin, we first determined if homologs remain paired after DSB induction. This was addressed by generating fly lines containing 256 LacO repeats next to the I-SceI cut site in the maternal homolog (LacO.I-SceI$_{cut}$) and 256 TetO repeats (without I-SceI cut site) in the paternal homolog (TetO), at the same genomic locus (one heterochromatic, two euchromatic integrations) (Fig. 5B). FISH with TetO and LacO probes showed that in actively dividing larval discs, the centroids of the TetO and LacO signals for both euchromatic and heterochromatic loci were separated by ~ 300nm, in the absence or presence of DSBs (γH2Av foci, Fig. 5C). Thus, homologs remain closely

associated after DSB induction, and could potentially be used as a template for HR in both eu- and hetero-chromatin.

We assessed the utilization of homologous sequences on either the sister chromatid (or *in cis* intrachromosomal templates) versus sequences on the homolog, by generating flies containing only the *iwhite* gene (i*white*_SNP) plus two silent SNPs (single nucleotide polymorphisms) inserted 15-basepairs up- and 13-basepairs down-stream of the I-SceI cut site respectively (Fig. 5D). Crossing i*white*_SNP flies with flies containing a DR-*white* integration at the exact same genomic locus results in progeny with *DR-white* on one homolog and *iwhite*_SNP on the other homolog (Fig. 5D). Recovery of DR-*white* HR products containing the SNPs identifies HR events with the homolog. We used specific amplification of the upstream *white* gene from DR-*white*/i*white*_SNP flies expressing ecDHFR.I-SceI and Sanger sequencing to determine the presence of HR sequences with and without the SNPs (Fig. 5D, E). This analysis revealed that the homolog is used in only 3-10% of all HR repair events, depending on the integration site (Fig. 5E). Illumina sequencing of the upstream *white* gene in repair products from one euchromatic (2eu_2) and one heterochromatic insertion (3het_1) produced the same frequencies observed with Sanger sequencing (Fig. 5F). We conclude that HR with the sister chromatid (or *in cis*) are strongly preferred for both heterochromatic and euchromatic DSBs, despite constitutive homolog pairing.

This led us to determine if the homolog might be favored as a template for HR repair in the absence of a sister chromatid. In most organisms there is limited HR in the G1 phase of the cell cycle, until S phase replication produces sister

chromatids (Ciccia and Elledge 2010). However, constitutive homolog pairing (McKee 2004) as well as the presence of many repetitive sequences in Drosophila heterochromatin suggests that HR repair could potentially occur in G0 or G1. To test this hypothesis, we compared the frequencies of DR-*white*/i*white*_SNP HR products in mitotically active larval brain to the adult brain, which is mostly composed of differentiated (G0/G1) cells (Fig. 5G). We heat-shock induced hsp70.I-SceI and harvested adult or larval brains 24 hours later. Strikingly, the proportion of repair events that utilized HR was significantly lower in the adult brain compared to larval brains, while the total amount of identified repair events were similar between the two tissues in 3 of 4 DR-*white* insertions tested (Fig.S5). One DR-*white* insertion (2het_1) showed a small, but significant, reduction in the total amount of repair products in adults (18%) compared to larval brains (23%), possibly reflecting a reduced induction of hsp70.I-SceI in adult brains, decreased DSB repair, or the use of an undetected alternative repair pathway. Nevertheless, HR is inhibited in G0/G1 cells that lack sister chromatids, despite the presence of paired homologs (Fig. 5G). The levels of HR in adult brains were below the detection limit needed to evaluate the presence of the SNPs (HR with the homolog), precluding comparisons with homolog HR frequencies determined for cycling larval tissues (Fig. 5E, F). We conclude that levels of HR with the homolog remain low in the G0 and G1 cell cycle phases, where we observe that NHEJ is the preferred pathway for DSB repair in both eu- and hetero-chromatic regions.

**Discussion**

Here we describe the successful integration and use of a single DSB system in Drosophila heterochromatin and euchromatin, which allowed us to analyze live DSB spatial dynamics and kinetics. To assess utilization of the two main repair pathways, HR and NHEJ, we also performed a detailed sequence analysis of DSB repair products from eu- and hetero-chromatic sites. We conclude that both chromatin regions employ these two repair pathways at similar frequencies, with NHEJ being the most prominent repair pathway utilized. In addition, we show that the homologous chromosome can be used as a template for HR repair, but sister chromatid (or *in cis*) sequences are preferred. Finally, HR levels drop significantly in differentiated adult brains, revealing similar cell cycle regulation in Drosophila as in many other organisms, independent of whether the DSB is located in hetero- or eu-chromatin.

Mobility of DSBs has been observed at both euchromatic and heterochromatic sites (Chiolo et al. 2013; Dion and Gasser 2013). However, the movement of heterochromatic foci is distinct. Heterochromatic DSBs initiate early repair events, then move outside the heterochromatin domain and ultimately associate with the nuclear periphery, where they recruit Rad51 and continue HR repair (Chiolo et al. 2011; Ryu et al. 2015). We observed that the movement of multiple heterochromatic DSBs induced by IR in cultured cells is also displayed by single DSBs in animal tissues. Thus, the distinct spatio-temporal responses at heterochromatic DSBs occur independently of the number or type of DSBs induced, and importantly occur in animal tissues, not only cultured cells. Furthermore, this

suggests that other damaging events induced by IR, such as oxidative stress, are not the main cause of heterochromatic DSB relocalization.

The observations that 1) the majority of heterochromatic DSBs are repaired by NHEJ, 2) 70% of breaks become associated with the heterochromatin periphery, and 3) repair foci movement was unaltered after either DmRad51, DmKu70 or DmCtIP depletion, suggest that DSB movement is not limited to breaks undergoing HR repair. We therefore propose that DSB relocalization is an intrinsic, global response for both HR and NHEJ repair in heterochromatin. We previously determined that canonical heterochromatin proteins are important for the peripheral movement of IR-induced DSBs (Chiolo et al. 2011), and it will be important to determine if DNA damage-specific changes to these proteins (e.g. post-translational modifications (PTMs) or complex composition) are involved in the movement of heterochromatic DSBs, and if the requirements differ for HR and NHEJ. Indeed, mammalian cell studies suggest that ATM-dependent phosphorylation of Kap1 is important for resolution of DSBs associated with heterochromatin, indicating that specific phosphorylation events could occur in different chromatin regions to promote repair (Goodarzi et al. 2008). In addition, this single break system will facilitate high temporal and spatial resolution imaging to elucidate the precise chromatin movements and proteins involved in DSB relocalization.

Although heterochromatic DSBs have been suggested to be repaired more slowly compared to euchromatic DSBs in mammals (Goodarzi et al. 2008), we observed no difference in mu2 repair foci kinetics (time from appearance to

disappearance) between eu- and hetero-chromatic DSBs (Fig. 2). Previous studies focused on IR-induced breaks (Goodarzi et al. 2008; Noon et al. 2010; Chiolo et al. 2011), which are known to create a variety of DSB ends and other types of DNA damage (Obe et al. 1992). It is therefore possible that these different types of DSB ends could require a longer time for repair, specifically in heterochromatic regions. In addition, the kinetics of break repair might also depend on the specific eu- and hetero-chromatic domains where the break is induced. Application of similar single break systems are needed to directly address the kinetics and regulation of repair responses in these distinct types of chromatin in mammals.

We previously identified a prominent role for HR in repair of heterochromatic breaks by observing an accumulation of IR-induced repair foci within heterochromatin after DmRad51 or DmRad54 knockdown in Drosophila cells, but not after DmKu70 or DmKu80 depletion (Chiolo et al. 2011). However, in this current study, using live mu2 foci analysis of single DSB breaks, we observed a delay in repair after DmRad51, DmCtIP or DmKu70 knockdown, demonstrating that both HR and NHEJ pathways play a role in the timely repair of heterochromatic breaks (Fig. 2). More importantly, DNA sequence analysis revealed that NHEJ is utilized more frequently than HR (~80% versus ~20%, respectively) for all tested hetero- and eu-chromatic DR-*white* insertions (Fig. 3).

A possible explanation for this difference is that our previous study used IR and fixed Drosophila cultured cells. The variety and multiple number of DNA breaks induced by IR (Obe et al. 1992) could require different repair pathways, and depend more on HR specifically in heterochromatin. In contrast, the relatively

simple single breaks produced by I-SceI are more similar to DSBs induced by replication fork collapse, and with limited processing might be more easily repaired by NHEJ. In addition, the percentage of cultured Drosophila cells in S and G2 is higher (>95% (Chiolo et al. 2011)) than in the larval tissues analyzed here (~50%, Fig. S1D, S4A), which could explain the observed differences in repair pathway utilization. Regardless, the more direct and extensive analyses presented here provides definitive evidence that repair of a simple DSB in whole tissues occurs via NHEJ more frequently than HR repair, for both euchromatic and heterochromatic DSBs.

Previous studies using DSB reporters in Drosophila have found relatively low levels of NHEJ utilization for DSB repair in euchromatic regions and high levels of SSA (Rong and Golic 2003; Preston et al. 2006; Johnson-Schlitz et al. 2007; Do et al. 2014). In addition, we identify a relatively low (3-10%) usage of the homolog as a template for HR (Fig. 5E,F), in contrast to a male germline repair study that identified ~45% of HR with the homolog (Rong and Golic 2003). One major difference between our study and other published studies is that the DR-*white* system introduces multiple *in cis* and *in trans* HR templates, which could compete with use of the homolog and reduce the number of identified HR events with the homolog.

Another important issue that can account for the observed differences in repair pathway dependency and homolog utilization is that here we mostly analyzed somatic cell repair products in the whole animal, in contrast to the exclusive focus on pre-meiotic male germline events in the other studies. Variations

in chromatin signatures as well as cell cycle differences in whole larvae versus pre-meiotic germline cells could account for different repair outcomes. In addition, all germline studies are limited to phenotypic analyses of offspring, which may not provide as much information as repair product sequence analysis.

Although we find that the majority of heterochromatic DSBs utilize either the HR or NHEJ pathway, we cannot rule out the involvement of other pathways in heterochromatin DSB repair. The percentage of identified SSA events in heterochromatin in germline repair experiments was relatively low (6-8%) and, comparable to euchromatic DSBs (Do et al. 2014)(Fig. S3A). Other studies using DSB repair reporters revealed a more prominent role for SSA in euchromatic DSB repair in Drosophila, ranging from 45 to 85% depending on the reporter (e.g., length of resection required for annealing), and repair templates present (Rong and Golic 2003; Preston et al. 2006; Johnson-Schlitz et al. 2007). The presence of an HR repair template in the vicinity of the DSB can efficiently compete with SSA for repair (Rong and Golic 2003). Therefore, the multiple HR repair templates present in the DR-*white* reporter system used here (Fig. 1A)(Do et al. 2014) could reduce SSA utilization, when compared to other reporter systems.

Nevertheless, in the absence of effective NHEJ or HR repair, alternative pathways such as SSA or Alt-NHEJ/MMEJ might become more important (Chan et al. 2010; Do et al. 2014; Ceccaldi et al. 2015). We observed that inhibition of NHEJ results in increased utilization of HR, without a decrease in the total number of repair events (Fig.4, S4). However, it is unclear if pathway 'switching' can occur when HR is inhibited, since depletion of DmRad51 and DmCtIP reduced the total

identified repair events in some but not all sequenced samples (Fig. S4B, C). Thus alternative repair pathways, whose products could not be identified with these methods, could repair DSBs in the absence of an active HR pathway. These alternative pathways are known to cause structural chromosomal changes (Chiruvella et al. 2013) and might therefore be more prone to induce aberrant repair products that could severely affect chromosome structure (e.g. dicentrics, acentrics). It will be of interest to analyze the role of alternative repair pathways in distinct chromatin regions, and to determine if there are differences with respect to aberrant repair in the absence of canonical HR and NHEJ pathways.

Our results require refinement of our model for how DSB spatio-temporal dynamics and heterochromatin proteins contribute to repairing heterochromatic DSBs in a manner that ensures genome stability. First, the demonstration in this study that homologs are infrequently utilized for HR repair, even in non-cycling cells, suggests that *in cis* (e.g. tandem repeats) or sister chromatid exchange events are more likely to be used for 'safe' HR repair. Second, the identification of a major role for NHEJ in heterochromatin DSB repair suggests an additional mechanism for ensuring genome stability. Specifically, NHEJ could circumvent the harmful chromosome aberrations that result from recombination between repeats on non-homologous chromosomes and avoid consequences of recombination with sister chromatid or *in cis* templates, that result in DNA loss or gain, and generation of extra chromosomal circles (Peng and Karpen 2007).

In sum, we have developed a targeted single break system in specific heterochromatic regions, and confirmed that single DSBs in heterochromatin

display similar spatio-temporal dynamics in *in vivo* larval tissue as previously observed for multiple DSBs after IR exposure in cultured cells. In addition, we have revealed a prominent role for both the NHEJ and HR repair pathways in DSB repair, independent of whether the break is induced in euchromatic or heterochromatic regions. Future research using this single break system will facilitate more detailed investigations of how DSB repair is regulated in these distinct nuclear compartments, including the roles of chromatin dynamics and developmental stages, and how disease states associated with genome instability are impacted by defects in heterochromatin DSB repair.

## Materials & Methods

### Fly lines and genotyping

Flies were grown at room temperature on standard medium, except where otherwise noted. Embryo injections and generation of DR-*white*, i*white*_SNP, LacO[256x].I-Sce$_{cut\text{-}site}$, TetO[256x], eYFP-mu2 and ecDHFR-HA.I-SceI fly lines were performed by BestGene Inc. (Chino Hills, CA, USA). An overview of the MiMIC integration sites and primers used for creating and genotyping DR-*white*, i*white*_SNP, LacO[256x].I-Sce$_{cut\text{-}site}$ and TetO[256x] fly lines are in Table S1. *yw* ; DR-*white*.y+ (DR-*white*_EC_2R1), *yw* ; hsp70.HA.I-Sce, Sco/CyO and *yw* ; + ; hsp70.HA.I-Sce,Sb/TM6B,Tb,Hu flies were previously described (Do et al. 2014). Transgenic fly lines expressing RFP-HP1a from its endogenous promoter were a kind gift from Dr. Hong Wen (Wen et al. 2008). RNAi lines used were UAS-DmKu70 RNAi (Bloomington #29594), UAS-DmRad51 RNAi (VDRC #13362), UAS-DmCtIP

(CG5872) RNAi (Bloomington # 36622 and VDRC #100035) and UAS.vermillion RNAi (Bloomington #50641). Act5C-Gal4 transgenes integrated on chromosome 2 (Bloomington #4414) or 3 (Bloomington #3954) were used for driving UAS.RNAi expression. Fly-FUCCI integrated on chromosome 3 (Bloomington #55124) was used for cell cycle analysis. Genotyping has been performed by lysing flies or larvae using the Phire Animal Tissue Direct kit (Thermo Fisher) according to manufacturers' guidelines. Information on the cloning of constructs and plasmids is in the online Supplemental Materials and Methods.

**DR-*white* repair analysis**

Quantification of germline DR-*white* repair products was performed as previously described (Do et al. 2014). SSA PCR was performed using primer sets described in Table S1. Quantification of somatic repair products in DR-*white*+ I-SceI+ larvae was performed by inducing I-SceI expression in larvae:

*ecDHFR system:* DR-*white* females were crossed with ecDHFR-I-SceI males on food containing Trimethoprim, which allows first through third instar DR-*white*; ecDHFR-I-SceI larval progeny to consume food containing 40μM trimethoprim and stabilize ecDHFR-I-SceI protein. Third instar DR-*white*; ecDHFR-I-SceI larvae were harvested and lysed for sequence analysis. To prepare food, 1 gram of Carolina Biological blue food (Formula 4-24 Instant Drosophila Medium, Blue) was mixed with 3ml of non-distilled water containing 3.2 μl of 100mM Trimethoprim while vortexing.

*Hsp70.I-SceI system:* DR-*white* females were crossed with hsp70.I-SceI males. The DR-*white*/hsp70.I-SceI second instar larvae were heat shocked for 1hr at 37°C, then harvested and lysed for sequence analysis after 24 hours. Detailed explanation of the sequencing analysis is in Supplemental Material and Methods.

**FISH, EdU and immunofluorescence staining**

For immunofluorescence (IF), FISH and IF-FISH stainings, imaginal discs were fixed as described previously (Dernburg 2012) and stored at -20°C in 95% ethanol. For all stainings, slides were thawed at room temperature and washed (dehydrated) in PBS for 20 minutes. Detailed protocols for IF, EdU staining, FISH and FISH-IF as well as the generation of FISH probes are in Supplemental Materials and Methods.

**Imaging**

Images of wing, leg or eye disc cells were acquired using a 60X oil immersion objective (NA 1.40) on a Deltavision microscope (Deltavision Spectris; Applied Precision, LLC) and images were deconvolved using SoftWoRx (Applied Precision, LLC). Time-lapse images were acquired once every 10 minutes. Image analysis and foci tracking of deconvolved images was performed manually using Fiji image analysis software.

For live mu2 foci tracking or Fly-FUCCI analysis, 3rd instar discs were pipetted on a slide in 10µl Schneider S1 medium supplemented with 10% FBS. A 22x22 mm no 1.5 coverslip (VWR) was placed on top of the discs, as described before (Lerit et al.

2014). For mu2 foci tracking the medium was supplemented with 400µM Trimethoprim.

**ChIP-qPCR**

Larvae were ground using mortar, pestle and liquid nitrogen. The powder was homogenized using a pestle A and B glass douncer in PBS 1mM EDTA pH 8.0. Fixation, nuclear extraction and sonication of third instar larval tissues were subsequently performed as described previously (Riddle et al. 2011). ChIP was performed as described elsewhere (O'Geen et al. 2011) using 3µg of H3K9me3 or H3K36me3 antibody and 2µg third instar larval chromatin. Enrichment for H3K9me3 and H3K36me3 was quantified by qPCR using Absolute Blue QPCR SYBR low ROX mix (Thermo-Fisher Scientific), and primers specific for the I-SceI [cut site] as well as the *yellow* (H3K9me3) or *rp49* (H3K36me3) gene as an internal control. qPCR was performed on the 7500 Fast Real-Time PCR system (Applied Biosystems). Primer sequences are in Table S1.

**RT-PCR**

RNA was isolated by homogenizing single larvae in 200µl Trizol. After 60µl chloroform addition and centrifugation, RNA from the aqueous phase was purified using an RNAeasy kit (Qiagen). cDNA was synthesized using Superscript III (Invitrogen) and oligo dT primers (IDT) following standard cDNA synthesis protocol (Invitrogen). PCR was subsequently performed on the cDNA with gene-specific primers (Table S1).

**Immuno Blotting**

Larvae were lysed in 30µl lysis buffer (20mM TrisHCl, 10mM KCl, 1.5mM MgCl2, 200mM NaCl, 0,1% NP40) for 30 minutes at 4°C and subsequently boiled for 5 minutes at 95°C in the presence of SDS loading buffer (5x diluted). 10µl of the total lysate was separated by SDS-page and transferred to Nitrocellulose membrane (Whatman), which were blotted with primary antibodies overnight at 4°C. Peroxidase-coupled or fluorescently labeled secondary antibodies and ECL (GE Healthcare) or Odyssey scanning (Li-cor) were used to visualize protein bands, respectively.

**Antibodies**

Primary antibodies used for WB were anti-DmKu70 (1:1000, rabbit, gift from Dr. Donald Rio), anti-DmRad51 (1:2000, rabbit, gift from Jim Kadonaga) and anti-tubulin (1:5000, mouse, Sigma). Primary antibodies used for IF were anti-HA (1:1000, mouse, ab130275), anti-γH2av (1:250, rabbit, Rockland or 1:250, mouse, DSHB UNC93-5.2.1), anti-Cyclin A (1:10, mouse, DSHB A12), anti-Serine 10 phospho Histone H3 (1:1000, rabbit, Upstate 06-570) and anti cleaved caspase3-Asp175 (1:500, rabbit, Cell Signaling, 9661). ChIP antibodies used were anti-H3K36me3 (rabbit, ab9050) and anti-H3K9me3 (rabbit, ab8898). Secondary antibodies used were Alexa 568 goat anti-rabbit or Alexa 488 goat anti-mouse for IF (1:500, Thermo-Fisher Scientific), goat anti-rabbit-HRP or goat anti-mouse-HRP

(1:10.000 ThermoScientific) for ECL, and donkey anti-mouse-680 or donkey anti-rabbit-800 (1:10.000 Li-cor) for use on the Odyssey (Li-cor).

**Acknowledgements**

These studies were supported by National Institutes of Health (NIH) R01 GM086613 to G.H.K, NIH grant 1R15GM110454-01 to J.R.L., the Dutch Cancer Society (KWF) - postdoctoral fellowship 2013-5854 to A.J. and the Netherlands Organization for Scientific Research - Rubicon fellowship 825.13.006 to A.J. The funders had no role in study design, data collection and analysis, decision to publish, or preparation of the manuscript.

Special thanks to all members of the Karpen, Dr. Priscilla Cooper and Dr. Sue Celniker labs for their invaluable input during lab meetings and project design.

**References**

Aymard F, Bugler B, Schmidt CK, Guillou E, Caron P, Briois S, Iacovoni JS, Daburon V, Miller KM, Jackson SP et al. 2014. Transcriptionally active chromatin recruits homologous recombination at DNA double-strand breaks. *Nature structural & molecular biology* **21**: 366-374.

Beucher A, Birraux J, Tchouandong L, Barton O, Shibata A, Conrad S, Goodarzi A, Krempler A, Jeggo P, Löbrich M. 2009. ATM and Artemis promote homologous recombination of radiation-induced DNA double-strand breaks in G2. *The EMBO journal* **28**: 3413-3427.

Brinkman EK, Chen T, Amendola M, van Steensel B. 2014. Easy quantitative assessment of genome editing by sequence trace decomposition. *Nucleic Acids Res* **42**: e168.

Burman B, Zhang ZZ, Pegoraro G, Lieb JD, Misteli T. 2015. Histone modifications predispose genome regions to breakage and translocation. *Genes Dev* **29**: 1393-1402.

Ceccaldi R, Liu JC, Amunugama R, Hajdu I, Primack B, Petalcorin MI, O'Connor KW, Konstantinopoulos PA, Elledge SJ, Boulton SJ et al. 2015. Homologous-recombination-deficient tumours are dependent on Poltheta-mediated repair. *Nature* **518**: 258-262.

Chan SH, Yu AM, McVey M. 2010. Dual roles for DNA polymerase theta in alternative end-joining repair of double-strand breaks in Drosophila. *PLoS Genet* **6**: e1001005.

Chen H, Zheng X, Zheng Y. 2014. Age-associated loss of lamin-B leads to systemic inflammation and gut hyperplasia. *Cell* **159**: 829-843.

Chiolo I, Minoda A, Colmenares SU, Polyzos A, Costes SV, Karpen GH. 2011. Double-Strand Breaks in Heterochromatin Move Outside of a Dynamic HP1a Domain to Complete Recombinational Repair. *Cell* **144**: 732-744.

Chiolo I, Tang J, Georgescu W, Costes SV. 2013. Nuclear dynamics of radiation-induced foci in euchromatin and heterochromatin. *Mutation research* **750**: 56-66.

Chiruvella KK, Liang Z, Wilson TE. 2013. Repair of double-strand breaks by end joining. *Cold Spring Harb Perspect Biol* **5**: a012757.

Cho U, Zimmerman SM, Chen LC, Owen E, Kim JV, Kim SK, Wandless TJ. 2013. Rapid and tunable control of protein stability in Caenorhabditis elegans using a small molecule. *PLoS One* **8**: e72393.

Ciccia A, Elledge SJ. 2010. The DNA damage response: making it safe to play with knives. *Mol Cell* **40**: 179-204.

Dernburg AF. 2012. Formaldehyde fixation of Drosophila tissues onto slides for whole-mount FISH. *Cold Spring Harb Protoc* **2012**.

Dion V, Gasser SM. 2013. Chromatin movement in the maintenance of genome stability. *Cell* **152**: 1355-1364.

Do AT, Brooks JT, Le Neveu MK, LaRocque JR. 2014. Double-strand break repair assays determine pathway choice and structure of gene conversion events in Drosophila melanogaster. *G3 (Bethesda)* **4**: 425-432.

Dronamraju R, Mason JM. 2009. Recognition of double strand breaks by a mutator protein (MU2) in Drosophila melanogaster. *PLoS Genet* **5**: e1000473.

Eissenberg JC, Elgin SC. 2000. The HP1 protein family: getting a grip on chromatin. *Current opinion in genetics & development* **10**: 204-210.

Ellinger J, Bachmann A, Goke F, Behbahani TE, Baumann C, Heukamp LC, Rogenhofer S, Muller SC. 2014. Alterations of global histone H3K9 and H3K27 methylation levels in bladder cancer. *Urol Int* **93**: 113-118.

Fodor BD, Shukeir N, Reuter G, Jenuwein T. 2010. Mammalian Su(var) genes in chromatin control. *Annu Rev Cell Dev Biol* **26**: 471-501.

Goodarzi AA, Jeggo PA. 2012. The heterochromatic barrier to DNA double strand break repair: how to get the entry visa. *International journal of molecular sciences* **13**: 11844-11860.

Goodarzi AA, Noon AT, Deckbar D, Ziv Y, Shiloh Y, Löbrich M, Jeggo PA. 2008. ATM signaling facilitates repair of DNA double-strand breaks associated with heterochromatin. *Molecular Cell* **31**: 167-177.

Heitz E. 1928. Das Heterochromatin der Moose. *Jahrb Wiss Bot*: 762-818.

Hoskins RA, Carlson JW, Wan KH, Park S, Mendez I, Galle SE, Booth BW, Pfeiffer BD, George RA, Svirskas R et al. 2015. The Release 6 reference sequence of the Drosophila melanogaster genome. *Genome Research* **25**: 445-458.

Jakob B, Splinter J, Conrad S, Voss KO, Zink D, Durante M, Lobrich M, Taucher-Scholz G. 2011. DNA double-strand breaks in heterochromatin elicit fast

repair protein recruitment, histone H2AX phosphorylation and relocation to euchromatin. *Nucleic Acids Res* **39**: 6489-6499.

Janssen A, Medema RH. 2013. Genetic instability: tipping the balance. *Oncogene* **32**: 4459-4470.

Jasin M. 1996. Genetic manipulation of genomes with rare-cutting endonucleases. *Trends Genet* **12**: 224-228.

Johnson RD, Jasin M. 2000. Sister chromatid gene conversion is a prominent double-strand break repair pathway in mammalian cells. *EMBO J* **19**: 3398-3407.

Johnson-Schlitz DM, Flores C, Engels WR. 2007. Multiple-pathway analysis of double-strand break repair mutations in Drosophila. *PLoS Genet* **3**: e50.

Kadyk LC, Hartwell LH. 1992. Sister chromatids are preferred over homologs as substrates for recombinational repair in Saccharomyces cerevisiae. *Genetics* **132**: 387-402.

Kharchenko PV, Alekseyenko AA, Schwartz YB, Minoda A, Riddle NC, Ernst J, Sabo PJ, Larschan E, Gorchakov AA, Gu T et al. 2011. Comprehensive analysis of the chromatin landscape in Drosophila melanogaster. *Nature* **471**: 480-485.

Lemaitre C, Grabarz A, Tsouroula K, Andronov L, Furst A, Pankotai T, Heyer V, Rogier M, Attwood KM, Kessler P et al. 2014. Nuclear position dictates DNA repair pathway choice. *Genes Dev* **28**: 2450-2463.

Lerit DA, Plevock KM, Rusan NM. 2014. Live imaging of Drosophila larval neuroblasts. *J Vis Exp*.

Liang F, Han M, Romanienko PJ, Jasin M. 1998. Homology-directed repair is a major double-strand break repair pathway in mammalian cells. *Proc Natl Acad Sci U S A* **95**: 5172-5177.

Mah LJ, El-Osta A, Karagiannis TC. 2010. gammaH2AX: a sensitive molecular marker of DNA damage and repair. *Leukemia* **24**: 679-686.

McKee BD. 2004. Homologous pairing and chromosome dynamics in meiosis and mitosis. *Biochimica et biophysica acta* **1677**: 165-180.

Nagel ZD, Margulies CM, Chaim IA, McRee SK, Mazzucato P, Ahmad A, Abo RP, Butty VL, Forget AL, Samson LD. 2014. Multiplexed DNA repair assays for multiple lesions and multiple doses via transcription inhibition and transcriptional mutagenesis. *Proc Natl Acad Sci U S A* **111**: E1823-1832.

Noon AT, Shibata A, Rief N, Löbrich M, Stewart GS, Jeggo PA, Goodarzi AA. 2010. 53BP1-dependent robust localized KAP-1 phosphorylation is essential for heterochromatic DNA double-strand break repair. *Nature cell biology* **12**: 177-184.

O'Geen H, Echipare L, Farnham PJ. 2011. Using ChIP-seq technology to generate high-resolution profiles of histone modifications. *Methods Mol Biol* **791**: 265-286.

Obe G, Johannes C, Schulte-Frohlinde D. 1992. DNA double-strand breaks induced by sparsely ionizing radiation and endonucleases as critical lesions for cell death, chromosomal aberrations, mutations and oncogenic transformation. *Mutagenesis* **7**: 3-12.

Peng JC, Karpen GH. 2007. H3K9 methylation and RNA interference regulate nucleolar organization and repeated DNA stability. *Nature cell biology* **9**: 25-35.

Peng JC, Karpen GH. 2009. Heterochromatic genome stability requires regulators of histone H3 K9 methylation. *PLoS Genetics* **5**: e1000435.

Peters AH, Carroll D, Scherthan H, Mechtler K, Sauer S, Schöfer C, Weipoltshammer K, Pagani M, Lachner M, Kohlmaier A et al. 2001. Loss of the Suv39h histone methyltransferases impairs mammalian heterochromatin and genome stability. *Cell* **107**: 323-337.

Preston CR, Flores CC, Engels WR. 2006. Differential usage of alternative pathways of double-strand break repair in Drosophila. *Genetics* **172**: 1055-1068.

Price BD, D'Andrea AD. 2013. Chromatin remodeling at DNA double-strand breaks. *Cell* **152**: 1344-1354.

Rangan P, Malone CD, Navarro C, Newbold SP, Hayes PS, Sachidanandam R, Hannon GJ, Lehmann R. 2011. piRNA production requires heterochromatin formation in Drosophila. *Current biology : CB* **21**: 1373-1379.

Riddle NC, Minoda A, Kharchenko PV, Alekseyenko AA, Schwartz YB, Tolstorukov MY, Gorchakov AA, Jaffe JD, Kennedy C, Linder-Basso D et al. 2011. Plasticity in patterns of histone modifications and chromosomal proteins in Drosophila heterochromatin. *Genome Research* **21**: 147-163.

Rogakou EP, Boon C, Redon C, Bonner WM. 1999. Megabase chromatin domains involved in DNA double-strand breaks in vivo. *J Cell Biol* **146**: 905-916.

Rong YS, Golic KG. 2003. The homologous chromosome is an effective template for the repair of mitotic DNA double-strand breaks in Drosophila. *Genetics* **165**: 1831-1842.

Ryu T, Spatola B, Delabaere L, Bowlin K, Hopp H, Kunitake R, Karpen GH, Chiolo I. 2015. Heterochromatic breaks move to the nuclear periphery to continue recombinational repair. *Nat Cell Biol* **17**: 1401-1411.

Schuster-Bockler B, Lehner B. 2012. Chromatin organization is a major influence on regional mutation rates in human cancer cells. *Nature* **488**: 504-507.

Soong CP, Breuer GA, Hannon RA, Kim SD, Salem AF, Wang G, Yu R, Carriero NJ, Bjornson R, Sundaram RK et al. 2015. Development of a novel method to create double-strand break repair fingerprints using next-generation sequencing. *DNA Repair (Amst)* **26**: 44-53.

Stucki M, Clapperton JA, Mohammad D, Yaffe MB, Smerdon SJ, Jackson SP. 2005. MDC1 directly binds phosphorylated histone H2AX to regulate cellular responses to DNA double-strand breaks. *Cell* **123**: 1213-1226.

Sulli G, Di Micco R, d'Adda di Fagagna F. 2012. Crosstalk between chromatin state and DNA damage response in cellular senescence and cancer. *Nat Rev Cancer* **12**: 709-720.

Venken KJ, Schulze KL, Haelterman NA, Pan H, He Y, Evans-Holm M, Carlson JW, Levis RW, Spradling AC, Hoskins RA et al. 2011. MiMIC: a highly versatile transposon insertion resource for engineering Drosophila melanogaster genes. *Nature methods* **8**: 737-743.

Weiler KS, Wakimoto BT. 1995. Heterochromatin and gene expression in Drosophila. *Annual review of genetics* **29**: 577-605.

Wen H, Andrejka L, Ashton J, Karess R, Lipsick JS. 2008. Epigenetic regulation of gene expression by Drosophila Myb and E2F2-RBF via the Myb-MuvB/dREAM complex. *Genes Dev* **22**: 601-614.
You Z, Bailis JM. 2010. DNA damage and decisions: CtIP coordinates DNA repair and cell cycle checkpoints. *Trends Cell Biol* **20**: 402-409.
Zielke N, Korzelius J, van Straaten M, Bender K, Schuhknecht GF, Dutta D, Xiang J, Edgar BA. 2014. Fly-FUCCI: A versatile tool for studying cell proliferation in complex tissues. *Cell Rep* **7**: 588-598.

**Figure legends**

**Figure 1. Inducible single break system for specific heterochromatic and euchromatic sites**

A) Schematic of the DR-*white* system. I-SceI expression produces a single DSB in the upstream *white* gene. Homologous recombination (HR) with the downstream, truncated *iwhite* sequence converts the 18-basepair I-SceI cut site to a wild-type *white* sequence (red eyes). White-eyed flies result from absence of an I-SceI-induced DSB, non-homologous end-joining (perfect NHEJ or NHEJ with processing), HR repair using the sister chromatid, or single strand annealing (SSA, with loss of the intervening 3xP3.dsRed marker), which can be analyzed in more detail by PCR and/or sequencing of repair products. B) Schematic of DR-*white* integrations in euchromatin (EC, eu) and heterochromatin (HC, het) on chromosomes 2, 3 and X. C) ChIP-qPCR analysis of H3K9me3 levels at the 9 DR-*white* insertions. The graph shows average H3K9me3 enrichment over input by qPCR (+ SD) of 3 experiments, using a primer set specific for the I-SceI cut site. H3K9me3 levels were standardized using a *yellow* qPCR primer set as an internal control (set at 1). D) Left: representative images of FISH staining for the AACAC heterochromatic repeat (red) and the DR-*white* locus (green) in 3rd instar larval discs with indicated

genotypes. Right: Quantification of FISH images. Each bar indicates average distance (nm) between the AACAC and DR-*white* centroids + SD. n ≥ 200 cells. ** p-value ≤ 1E-22, two-tailed unpaired student *t*-test. E) Schematic of two inducible I-SceI expression systems. 1) ecDHFR-I-SceI degradation through proteolysis is blocked upon addition of the stabilizing ligand Trimethoprim. 2) The hsp70 promoter upstream of the I-SceI gene is activated by shifting to 37°C for 1hr. RT = room temperature. F) Top: representative images of IF staining for γH2Av (green) in 3rd instar larval wing disc cells. DAPI (blue) = DNA. Bottom: Quantification of the percentages (+ SD) of nuclei that contain one γH2Av focus is plotted for samples treated for 3h with the DMSO control (black bars) or Trimethoprim (grey bars). n ≥ 4 independent experiments, ≥500 wing or leg disc cells each,. *p-value ≤ 0.05, ** p-value ≤ 0.002, n.s. = significant (p = 0.2), two-tailed unpaired student *t*-test.

**Figure 2. Live imaging of single break dynamics in euchromatin and heterochromatin**

A) Left: representative images of mu2-YFP foci dynamics (green) with respect to the HP1a domain (red) in larval wing disc cells. The three most common categories of mu2 foci dynamics are shown: 1) arise and resolve outside of the HP1a domain (top), 2) arise inside the HP1a domain and move to the periphery (middle), and 3) arise and resolve at the HP1a periphery (bottom). Right: Quantification and categorization of single mu2 foci dynamics. Bars indicate the average percentage (+ SD) of 3 independent experiments per DR-*white* insertion, n=30 cells of leg and wing discs were imaged per experiment. B) Time-lapse analysis of single mu2-YFP-

foci disappearance (minutes from appearance) in 3rd instar larval leg and wing discs treated as in A). The time point of mu2 focus appearance was set at t=0 for each individual focus. n = number of DR-*white* insertions imaged for either HC or EC, at least 90 cells (= single mu2 foci) were analyzed per insertion, error bars = + SEM. n.s.: p-value = 0.2295, log-rank (Mantel-Cox) test. Dashed line indicates the time it took for 50% of mu2 foci to disappear. C) Lysates from Actin-GAL4 expressing (-) or Actin-GAL4 and UAS. DmRad51 (left) or UAS.DmKu70 RNAi (middle) expressing 3rd instar larvae were immunoblotted for tubulin, and DmRad51 (left) or DmKu70 (middle). Right: RT-PCR with DmCtIP and actin specific primers on RNA from 3rd instar larvae expressing Actin-GAL4 (-) or Actin-GAL4 and UAS.DmCtIP RNAi. D, E) Wing and leg disc cells with indicated RNAi depletions were imaged in the presence (black lines, GAL4 only) or absence of either DmRad51 (grey line, left graphs), DmCtIP (blue line, left graphs) or DmKu70 (grey line, right graphs) as in B. n= number of cells imaged per condition. ** p-value < 0.0001, log-rank (Mantel-Cox) test. Different EC and HC DR-*white* integrations were imaged with DmRad51/DmCtIP or DmKu70 RNAi due to genetic limitations. Dashed lines indicate the time it took for 50% of mu2 foci to disappear.

**Figure 3. Sequence analysis of repair products reveals utilization of both HR and NHEJ pathways in heterochromatin and euchromatin**

A) Left: Schematic of crosses performed for DR-*white* germline repair product analysis. 0-3 day old DR-*white*/hsp70.I-SceI embryos and larvae were heat shocked for 1 hour at 37°C to induce I-SceI expression and single DSBs, then allowed to

develop into adults. Male DR-*white*/hsp70.I-SceI adults with mosaic *white* expression were crossed to *white* mutant (-) females, and F1 progeny were analyzed for eye color. Right: Percentage of red-eyed (*white*+) F1 progeny (HR events) in the germline and is plotted for indicated DR-*white* insertions. n ≥ 7 F0 DR-*white*/hsp70.I-SceI males per DR-*white* insertion. B) Illumina sequencing of the upstream *white* PCR product from genomic DNA of indicated DR-*white*/ecDHFR-I-SceI larvae that were fed Trimethoprim. Percentage of reads with insertions and deletions (NHEJ, grey bars) or HR products (HR, black bars) over the total pool of reads of detectable repair products are plotted. Bars indicate average percentages + SD of 2 independent experiments (larvae) per condition. C) Quantification of the percentage of NHEJ products with deletions (black) or insertions (grey) identified by Illumina sequencing for indicated DR-*white* insertions. Bars indicate average percentages + SD of 2 independent experiments (larvae) per condition.

**Figure 4. Hetero- and eu-chromatic DSB repair utilize both NHEJ and HR pathways**

A-C) Quantification of the relative ratio of HR products over total identified repair products (+ SEM) using the TIDE-algorithm in the presence (black bars, GAL4 only) or absence (grey bars, GAL4 + UAS.RNAi) of DmKu70 (A), DmRad51 (B) or DmCtIP (C). n ≥ 3 DR-*white*/I-SceI larvae per condition. *p-value ≤0.04, ** p-value ≤ 0.009, p-values indicate values from two-tailed unpaired student *t* test.

**Figure 5. Recombination with the homologous chromosome**

A) Schematic of homolog pairing in *Drosophila* in the G1/S/G2 phases of the cell cycle. B) Top: Schematic of the LacO.I-SceI[cut-site]/TetO system. 256xLacO.I-SceI[cut-site] (red) insertion on one homolog and 256xTetO (blue) on the other homolog allows for the visualization of the two homologs. Bottom: Representative images of 3rd instar leg disc cells stained with LacO (red) and TetO (blue) FISH probes in combination with γH2Av (green) immunofluorescence in the absence (- γH2Av) and presence (+ γH2Av) of a single DSB. C) Quantification of images as shown in B. Distance (nm) between the LacO and TetO FISH centroids is shown in the absence (- γH2Av in LacO, grey dots) or presence of a single DSB (+ γH2Av in LacO, red dots). One dot represents one cell with a LacO and TetO signal. n ≥ 50 cells per condition. Black line indicates mean +/- SEM. n.s. is not significant (p-value ≥ 0.11), unpaired two-tailed student *t*-test. D) HR with the sister chromatid or *in cis* (intrachromosomal) in the DR-*white*/i*white* SNP system results in a wild-type *white* gene (top). HR with the homolog in the DR-*white*/i*white*_SNP system results in a *white* gene containing one or two SNPs, which are 15 basepairs upstream and 13 basepairs downstream of the *iwhite* site homologous to the I-SceI cut site. E) Quantification of the percentage of HR products with SNPs (HR with the homolog) of the total pool of HR sequences (+ SEM) using TIDE-Sanger sequencing analysis of indicated DR-*white*/i*white*_SNP integrations. n ≥ 6 flies/condition. F) Quantification of the number of reads containing HR products with SNPs (HR with the homolog, red) and wild type *white* (HR with sister or *in cis*, black) by Illumina sequencing (+ SD). n=2 larvae/condition. G) Top: Schematic representation of single DSB induction in larval (top) and adult (bottom) brain. 24 hours after heat shock

induction of hsp70.I-SceI, brains were processed for PCR amplification and Sanger sequence analysis using TIDE. Bottom: Bars represent the average ratio of HR products over total identified repair products of 3 independent experiments (+ SEM) for larval (black) and adult brains (grey) with indicated DR-*white* insertions. n ≥ 3 brains/condition. ** p-value ≤ 0.0012, unpaired two-tailed student *t* test.

**Supplemental Material:**

- Supplemental Fig. S1-5
- Supplemental Table S1
- Supplemental Materials & Methods Fig.1
- Supplemental Materials & Methods text

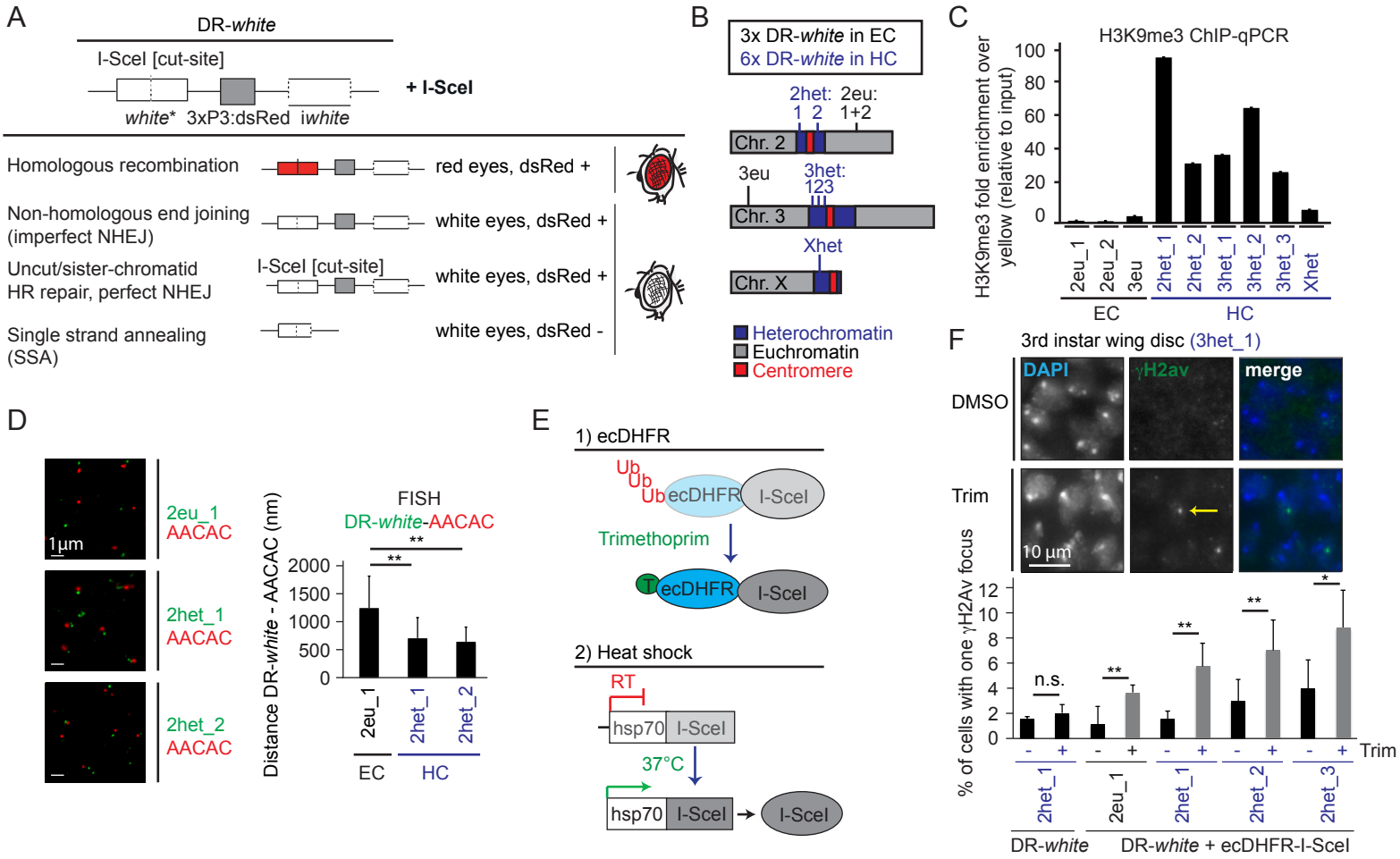
A
DR-white
I-SceI [cut-site]
+ I-SceI
white* 3xP3:dsRed iwhite
Homologous recombination
red eyes, dsRed +
Non-homologous end joining (imperfect NHEJ)
white eyes, dsRed +
Uncut/sister-chromatid HR repair, perfect NHEJ
I-SceI [cut-site]
white eyes, dsRed +
Single strand annealing (SSA)
white eyes, dsRed -
B
3x DR-white in EC
6x DR-white in HC
2het: 2eu:
1 2 1+2
Chr. 2
3eu
3het:
123
Chr. 3
Xhet
Chr. X
Heterochromatin
Euchromatin
Centromere
C
H3K9me3 ChIP-qPCR
H3K9me3 fold enrichment over yellow (relative to input)
100
80
60
40
20
0
2eu_1
2eu_2
3eu
2het_1
2het_2
3het_1
3het_2
3het_3
Xhet
EC
HC
D
1µm
2eu_1 AACAC
2het_1 AACAC
2het_2 AACAC
FISH
DR-white-AACAC
Distance DR-white - AACAC (nm)
2000
1500
1000
500
0
**
**
2eu_1
2het_1
2het_2
EC
HC
E
1) ecDHFR
Ub
Ub
Ub
ecDHFR
I-SceI
Trimethoprim
T
ecDHFR
I-SceI
2) Heat shock
RT
hsp70
I-SceI
37°C
hsp70
I-SceI
I-SceI
F
3rd instar wing disc (3het_1)
DAPI
γH2av
merge
DMSO
Trim
10 µm
% of cells with one γH2Av focus
12
10
8
6
4
2
0
n.s.
**
**
**
*
- + - + - + - + - +
Trim
2het_1
2eu_1
2het_1
2het_2
2het_3
DR-white
DR-white + ecDHFR-I-SceI

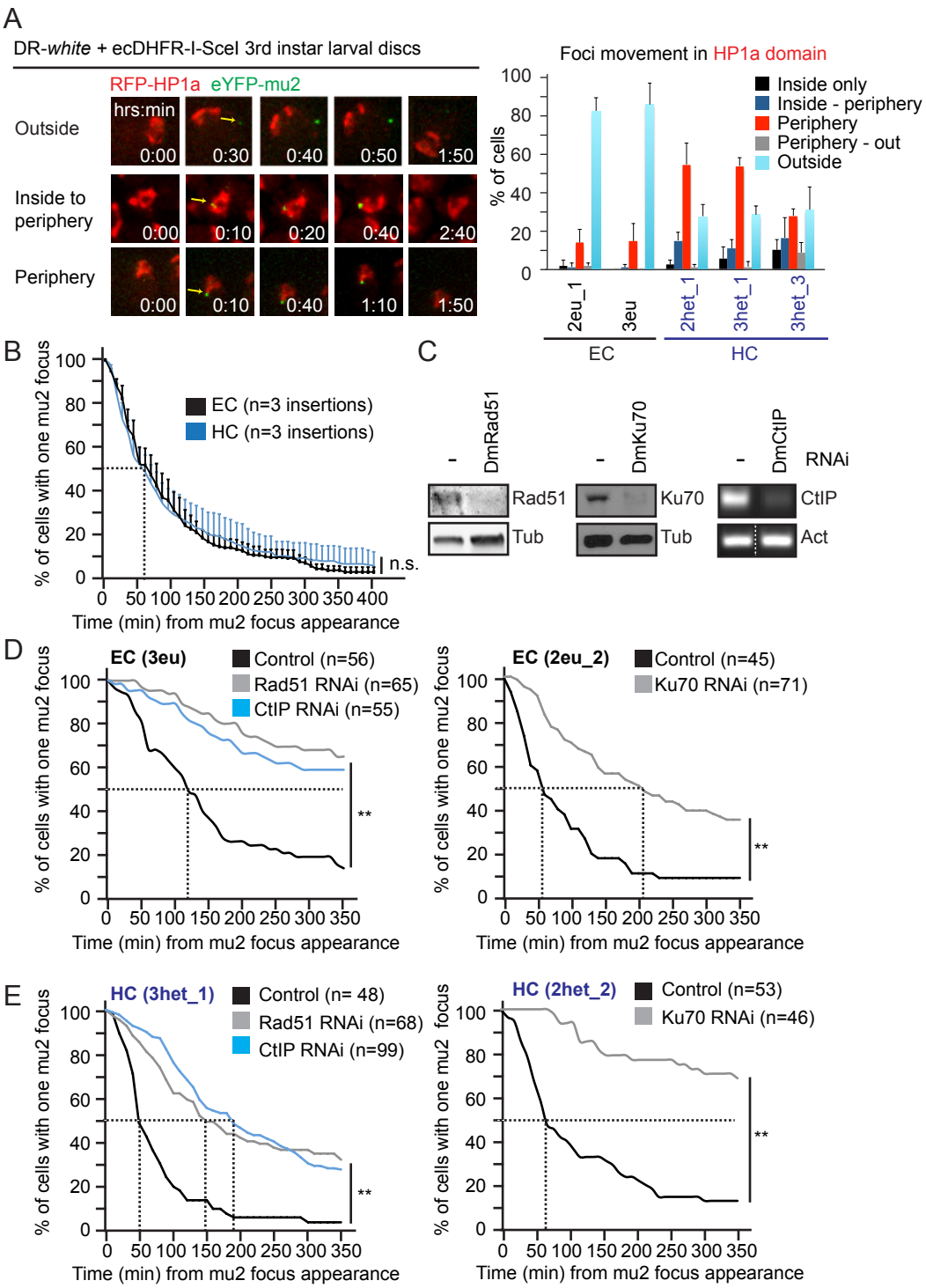
A
DR-white + ecDHFR-I-SceI 3rd instar larval discs
RFP-HP1a eYFP-mu2
Outside
Inside to periphery
Periphery
hrs:min
0:00
0:30
0:40
0:50
1:50
0:10
2:40
1:10
Foci movement in HP1a domain
% of cells
Inside only
Inside - periphery
Periphery
Periphery - out
Outside
2eu_1
3eu
2het_1
3het_1
3het_3
EC
HC
B
% of cells with one mu2 focus
EC (n=3 insertions)
HC (n=3 insertions)
n.s.
Time (min) from mu2 focus appearance
C
DmRad51
DmKu70
DmCtIP
RNAi
Rad51
Ku70
CtIP
Tub
Act
D
EC (3eu)
Control (n=56)
Rad51 RNAi (n=65)
CtIP RNAi (n=55)
EC (2eu_2)
Control (n=45)
Ku70 RNAi (n=71)
**
E
HC (3het_1)
Control (n= 48)
Rad51 RNAi (n=68)
CtIP RNAi (n=99)
HC (2het_2)
Control (n=53)
Ku70 RNAi (n=46)

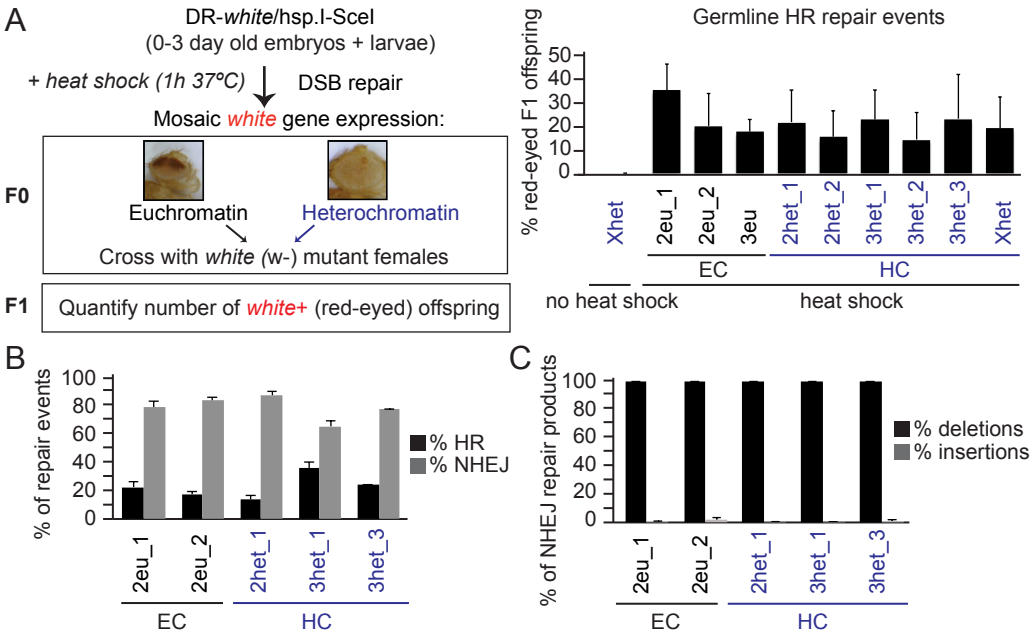
A
DR-white/hsp.I-SceI
(0-3 day old embryos + larvae)
+ heat shock (1h 37°C)
DSB repair
Mosaic white gene expression:
F0
Euchromatin
Heterochromatin
Cross with white (w-) mutant females
F1
Quantify number of white+ (red-eyed) offspring
Germline HR repair events
% red-eyed F1 offspring
50
40
30
20
10
0
Xhet
2eu_1
2eu_2
3eu
2het_1
2het_2
3het_1
3het_2
3het_3
Xhet
EC
HC
no heat shock
heat shock
B
% of repair events
100
80
60
40
20
0
% HR
% NHEJ
2eu_1
2eu_2
2het_1
3het_1
3het_3
EC
HC
C
% of NHEJ repair products
100
80
60
40
20
0
% deletions
% insertions
2eu_1
2eu_2
2het_1
3het_1
3het_3
EC
HC

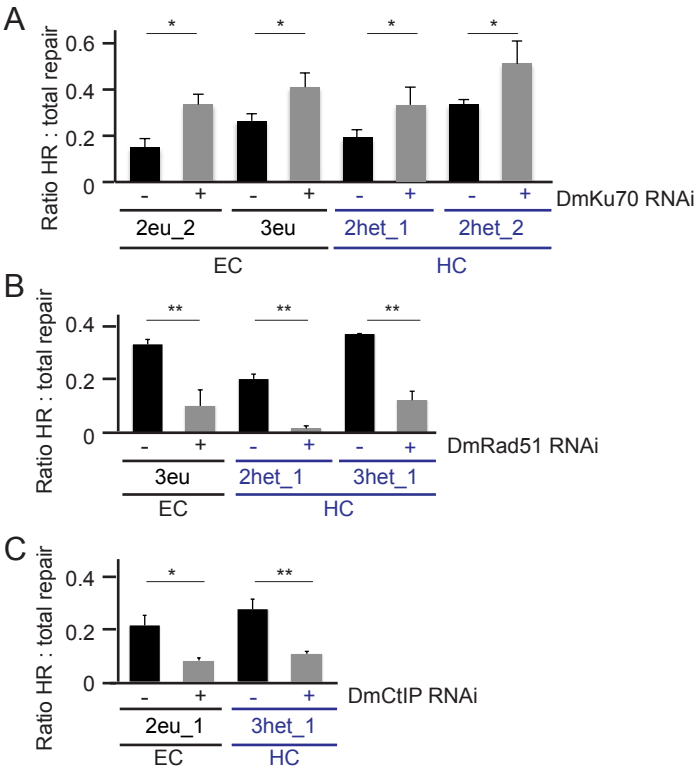
A
Ratio HR : total repair
0.6
0.4
0.2
0
*
*
*
*
- + - + - + - +
DmKu70 RNAi
2eu_2
3eu
2het_1
2het_2
EC
HC
B
Ratio HR : total repair
0.4
0.2
0
**
**
**
- + - + - +
DmRad51 RNAi
3eu
2het_1
3het_1
EC
HC
C
Ratio HR : total repair
0.4
0.2
0
*
**
- + - +
DmCtIP RNAi
2eu_1
3het_1
EC
HC

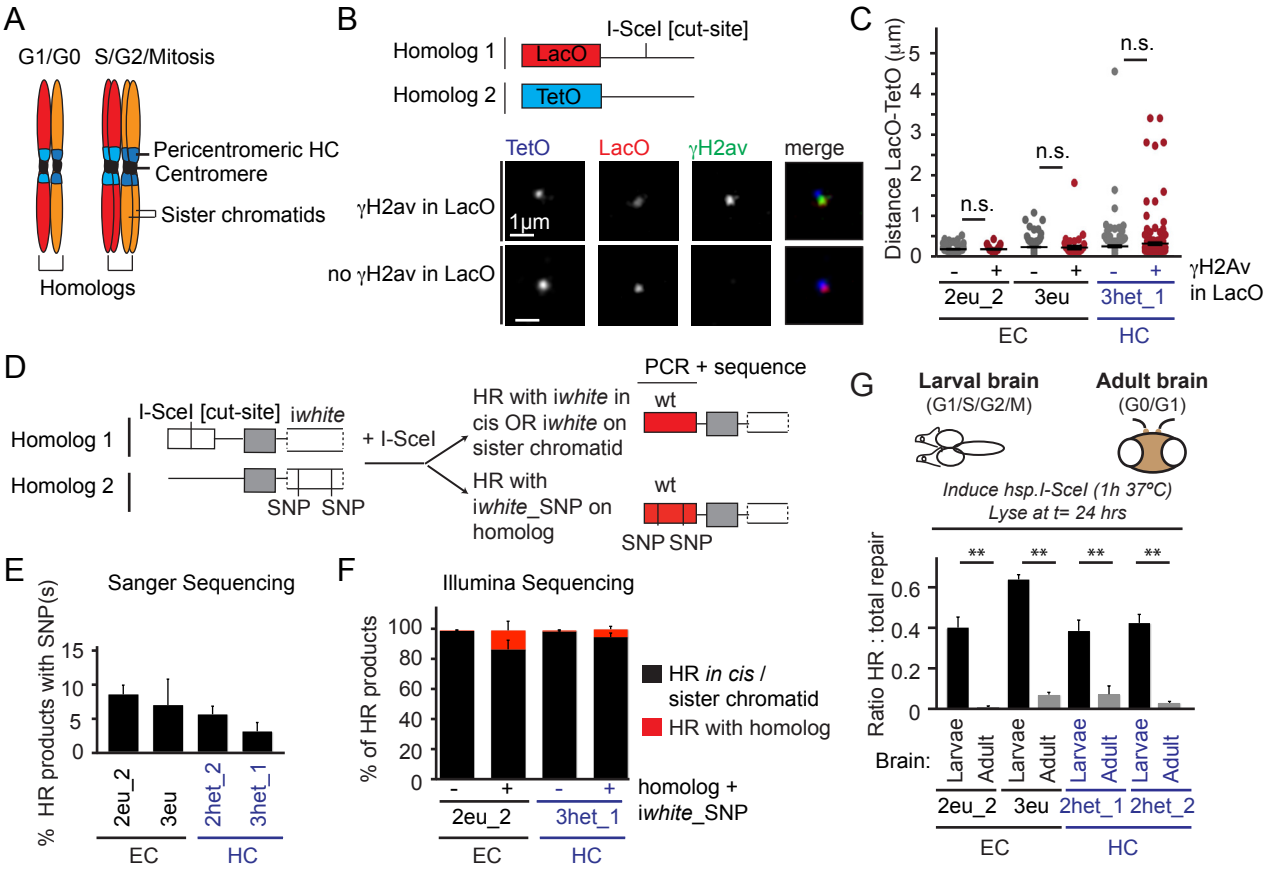
A
G1/G0
S/G2/Mitosis
Pericentromeric HC
Centromere
Sister chromatids
Homologs
B
I-SceI [cut-site]
Homolog 1
LacO
Homolog 2
TetO
TetO
LacO
γH2av
merge
γH2av in LacO
no γH2av in LacO
1μm
C
Distance LacO-TetO (μm)
n.s.
n.s.
n.s.
γH2Av in LacO
2eu_2
3eu
3het_1
EC
HC
D
I-SceI [cut-site]
iwhite
Homolog 1
Homolog 2
SNP SNP
+ I-SceI
PCR + sequence
HR with iwhite in cis OR iwhite on sister chromatid
wt
HR with iwhite_SNP on homolog
wt
SNP SNP
E
Sanger Sequencing
% HR products with SNP(s)
2eu_2
3eu
2het_2
3het_1
EC
HC
F
Illumina Sequencing
% of HR products
HR in cis / sister chromatid
HR with homolog
homolog + iwhite_SNP
2eu_2
3het_1
EC
HC
G
Larval brain
(G1/S/G2/M)
Adult brain
(G0/G1)
Induce hsp.I-SceI (1h 37°C)
Lyse at t= 24 hrs
Ratio HR : total repair
Brain:
Larvae
Adult
2eu_2
3eu
2het_1
2het_2
EC
HC

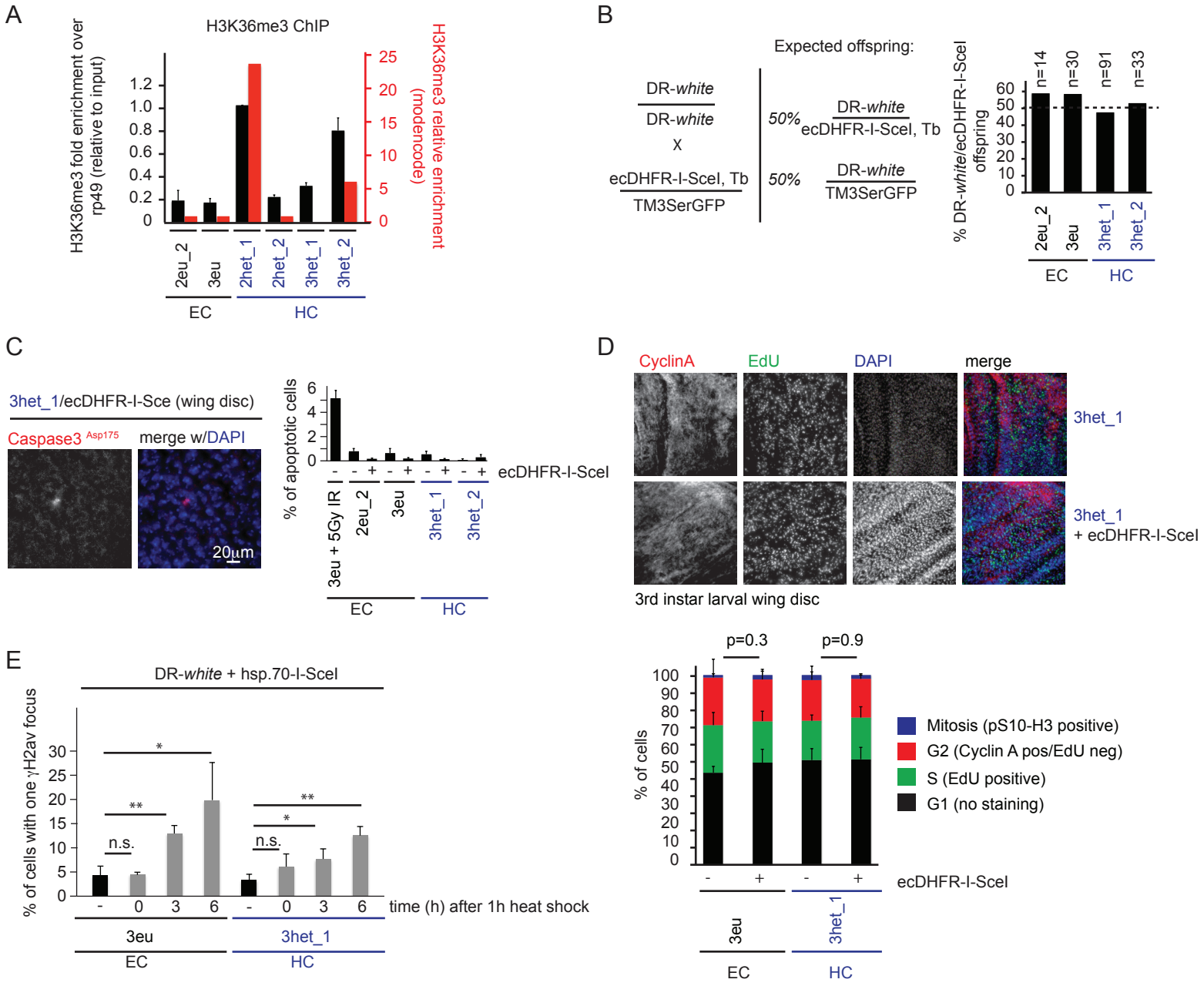


**Supplemental figure 1 (related to figure 1)**

A) Left (black bars): ChIP-qPCR analysis of H3K36me3 levels at the indicated DR-*white* insertions. The graph shows H3K36me3 enrichment over input examined by qPCR using a primer set specific for the I-SceI cut site. H3K36me3 levels were standardized using a rp49 qPCR primer as an internal positive control (set at 1). n=3 qPCR experiments + SD for each DR-*white* insertion. Right (red bars): relative H3K36me3 enrichment at the original genetic loci (no DR-*white* insertions) as determined by the Modencode project in 3rd instar wildtype larvae (gbrowse.modencode.org). B) Quantification of the percentage of DR-*white*/ecDHFR-I-SceI larval offspring as a measure of ecDHFR-I-SceI induced organismal lethality. n= total number of 3rd instar larval offspring from the indicated DR-*white*/DR-*white* X ecDHFR-I-SceI, Tb/TM3SerGFP crosses fed with Trimethoprim. Dotted line indicates the expected 50% of DR-*white*/ecDHFR-I-SceI larvae in the absence of any organismal lethality. C) The percentage of apoptotic cells was determined in 3rd instar larval DR-*white* wing discs using an antibody against cleaved caspase 3, four hours after 5Gy IR (positive control) or in the absence (-) or presence (+) of ecDHFR-I-SceI expression. n=3 wing discs per condition. Average + SD is plotted. D) Cell cycle analysis upon Trim feeding of larvae in the absence or presence of the ecDHFR-I-SceI transgene. Top: representative images of larval wing discs treated with EdU (green), stained with an antibody recognizing Cyclin A (red) and DAPI (blue) to mark nuclei. Bottom: quantification of images as shown above. Average percentages were calculated of cells in S (EdU positive), G2 (Cyclin A positive, EdU negative) or G1 phase (no staining). Mitotic cells were assessed in the same discs using an antibody recognizing phospho-Serine10-Histone H3 (not shown in image). n= 3 wing discs per condition + SD with at least 400 cells counted per disc. p-values were calculated by comparing the percentage of G1 cells between indicated samples with the student t-test, unpaired, two-tailed. E) Quantification of γH2av IF staining as shown in Fig.1F. Wing and leg discs from hsp70.I-SceI third instar larvae with indicated DR-*white* insertions were dissected and fixed 0, 3, and 6 h after heat shock (grey bars). Non-heat shocked tissue was used as a control (black bars). n = 3 independent experiments with each ≥ 120 cells + SD. n.s. not significant ($p \geq 0.16$), * p-value ≤ 0.04, ** p-value ≤ 0.003, student t-test, unpaired, two-tailed.

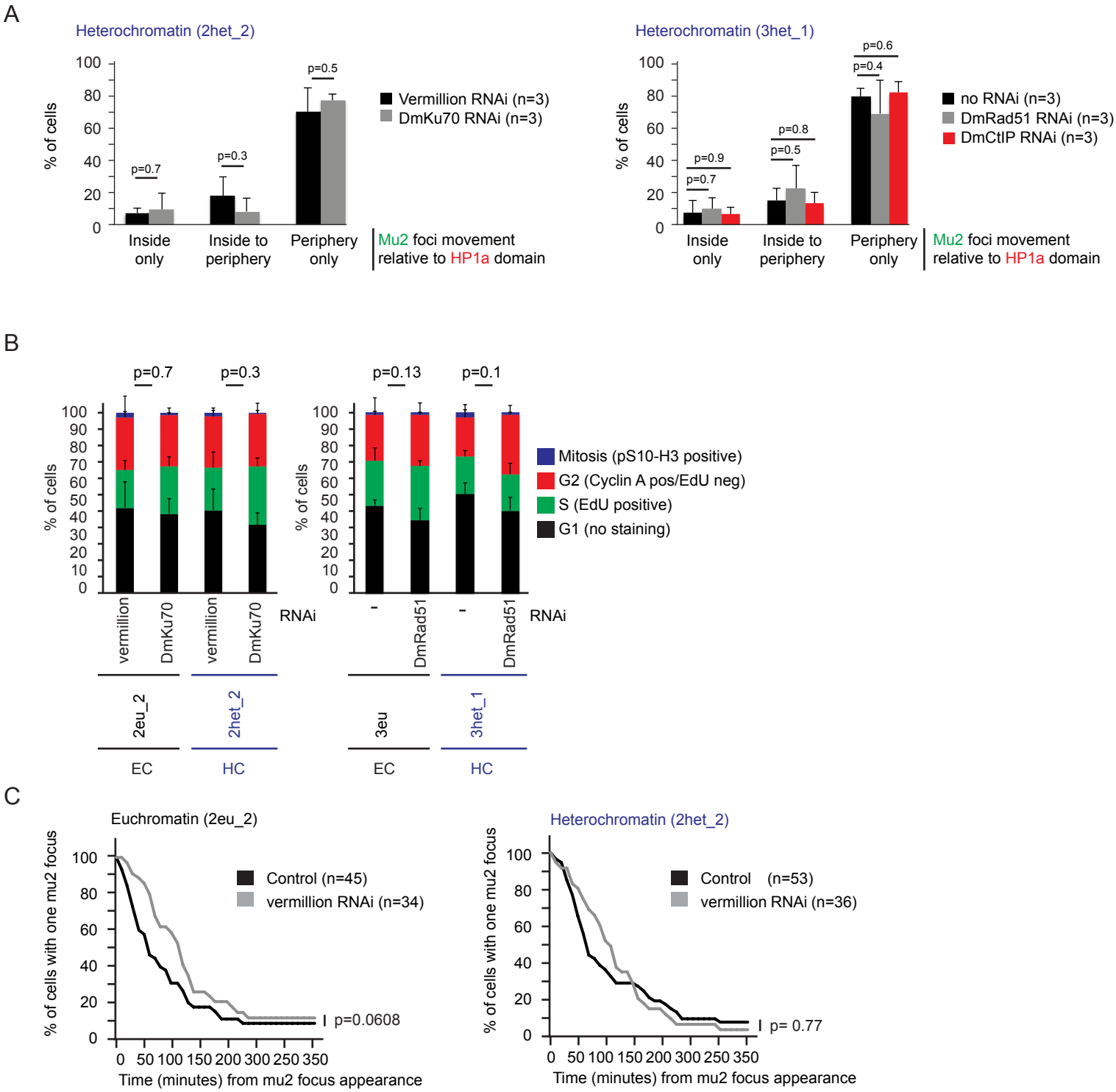


**Supplemental figure 2 (related to figure 2)**

A) Quantification of mu2 foci movement as in Fig.2A in leg and wing discs with indicated DR-*white* insertions. Foci movement was determined in the presence of vermillion (control) and DmKu70 RNAi (left) or no (GAL4 only), DmRad51 or DmCtIP RNAi (right). Only three categories are shown: 'inside only': mu2 foci arise and disappear within the HP1a domain without apparent peripheral movement. 'inside to periphery': mu2 foci come up in the HP1a domain and move to the periphery of the domain. 'periphery only': foci arise and disappear at the HP1a periphery. Averages + SD are shown of 3 independent experiments with each at least 30 cells imaged. p-values were calculated using student t-test, unpaired, two-tailed. B) Cell cycle analysis as in Fig.S1D of 3rd instar DR-*white* larval wing discs in the absence (-) or presence of GAL4 driven vermillion, DmKu70 or DmRad51 RNAi. p-values were calculated by comparing the percentage of G1 cells between samples with the student t-test, unpaired, two-tailed. Average +SD of n=3 wing discs per sample with > 400 cells counted per disc.C) Cells of 3rd instar wing and leg discs with indicated DR-*white* insertions were imaged and quantified as in Fig.2B in the absence (GAL4 only) and presence of vermillion RNAi. n= number of cells imaged. p-values were calculated with the log-rank (Mantel-Cox) test.

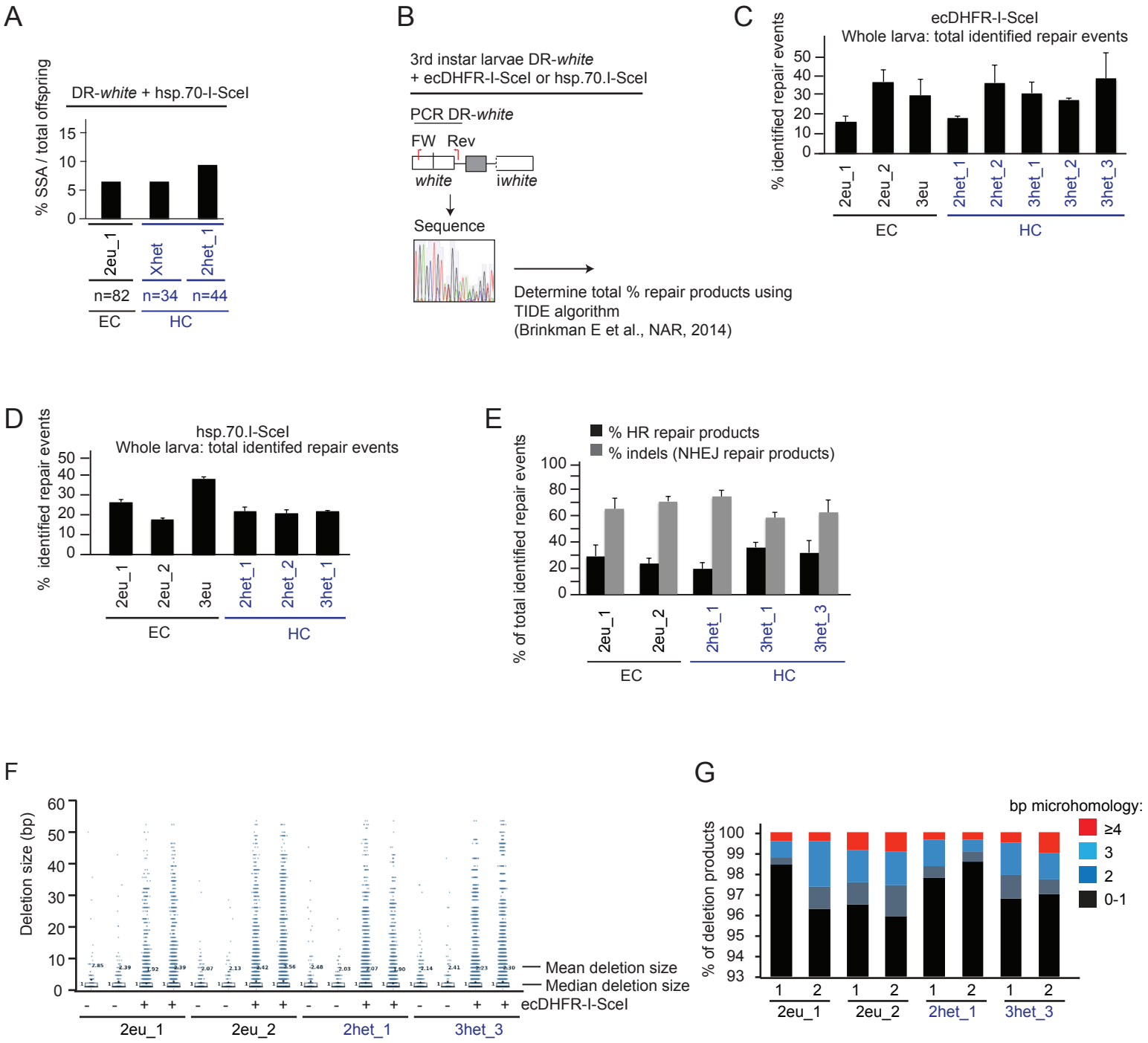


**Supplemental figure 3 (related to figure 3)**

A) Quantification of the percentage of germline SSA repair events of the total number of offspring. I-SceI was induced in DR-*white*/hsp70.I-SceI embryos as described in Fig. 3A and {Do, 2014 #1087}. PCR amplification was performed on genomic DNA of white-eyed, 3xp3-dsRed negative progeny using an SSA-specific primer set ((Do et al., G3, 2014) and Table S1) to quantify the number of germline SSA events. n = number of total F1 offspring analyzed. B) I-SceI expression was induced in DR-*white*/I-SceI larvae. PCR was performed on genomic DNA of single larvae to amplify the upstream white gene. C, D) TIDE-algorithm dependent Sanger sequence analysis (0-100 base pairs downstream from I-SceI cut site) (Brinkman et al., 2014) reveals an increase in repair products at the I-SceI cut site for indicated DR-*white* insertions processed as in B with either ecDHFR-I-SceI (C) or hsp70.I-SceI (D) induction. n ≥ 3 DR-white/I-SceI larvae per condition + SEM. E) TIDE algorithm-dependent extraction of the percentage of HR products (black bars) and insertions and deletions (indels) (grey bars) from the total pool of DNA repair products identified as in B-D using Sanger Sequencing. PCR was performed on genomic DNA from larvae with indicated DR-white/ecDHFR.I-SceI insertions. n ≥ 3 DR-white/I-SceI larvae per condition + SEM. F) Quantification of the size of deletions (basepairs) identified by Illumina sequencing as performed in Fig. 3B in indicated DR-*white* larval samples. One dot indicates one sequencing read with a deletion product. All larvae (-/+ ecDHFR-I-SceI transgene) were fed with Trimethoprim. G) Quantification of the percentage of deletion products in F) with 0-1, 2, 3 and 4 or more basepair microhomology identified by Illumina sequencing in individual DR-*white* larval samples + I-SceI. Individual samples are displayed (1,2).

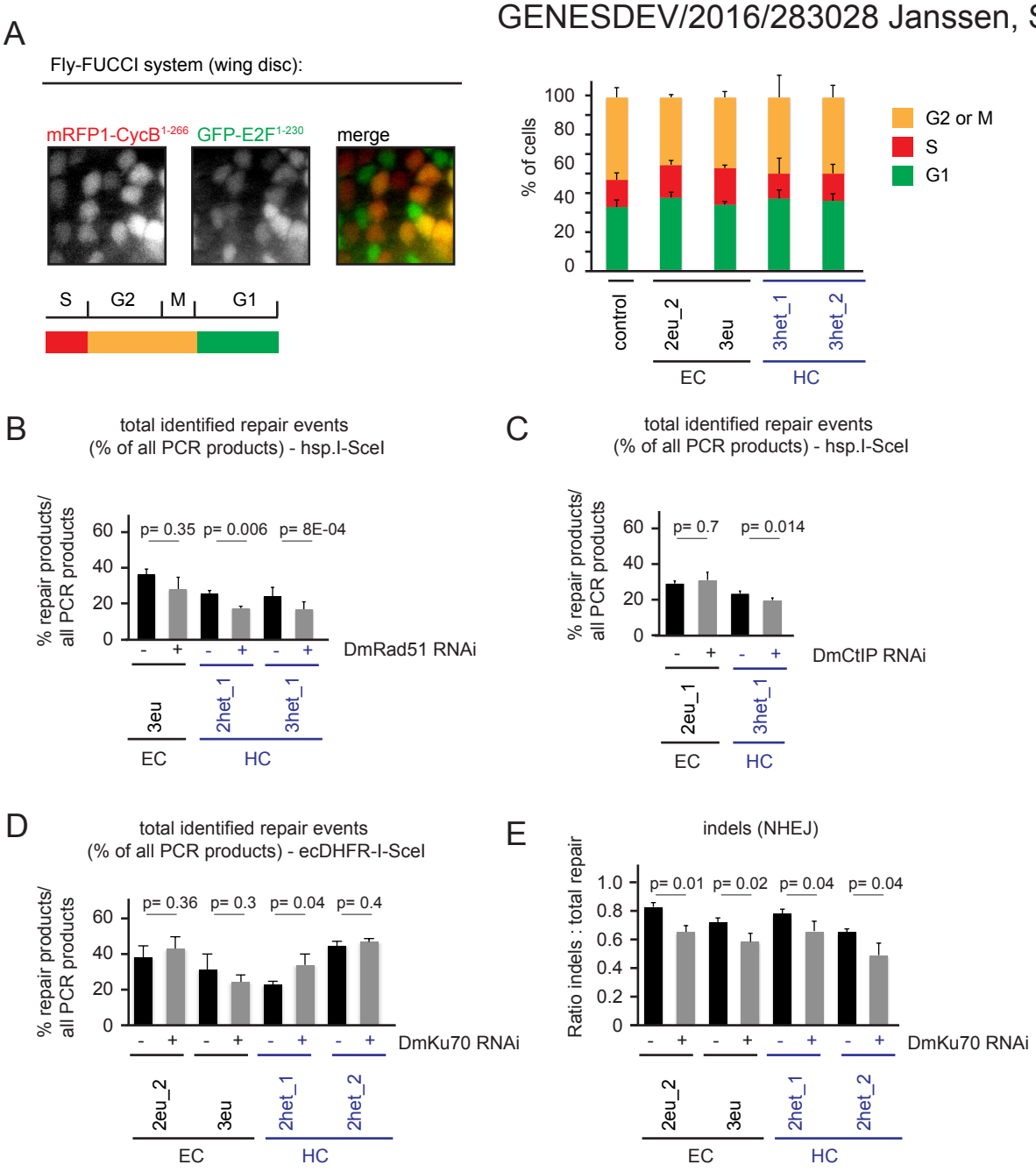


**Supplemental figure 4 (related to figure 4)**

A) Left: Representative images of the Fly-FUCCI system in wing discs. Right: Cell cycle analysis using the Fly-FUCCI system as shown on the left in wing discs of 3rd instar larvae with control (FUCCI only) or FUCCI + indicated DR-*white* integrations. n= 3 wing discs per condition + SD with at least 200 cells counted per disc. p-values were calculated by comparing the percentage of G1 cells between control FUCCI discs and indicated samples (2eu_2 (p=0.14), 3eu (p=0.59), 3het_1 (p=0.27), 3het_2(p=0.34)) using the student t-test, unpaired, two-tailed. B-D) Quantification as in Fig.S3B-D of the percentage of TIDE-identified repair products from the total pool of PCR products in the presence (black bars, GAL4 only) or absence (grey bars, GAL4 + UAS.RNAi) of DmRad51 (B), DmCtIP (C) or DmKu70 (D). E) Quantification of the ratio of NHEJ (indels) products (of the total pool of identified repair products) in the presence (black bars, GAL4 only) or absence (grey bars, GAL4 + UAS.RNAi) of DmKu70. p-values were calculated using the two-tailed, unpaired student t-test. Averages are shown of n ≥ 3 larvae per condition + SD.

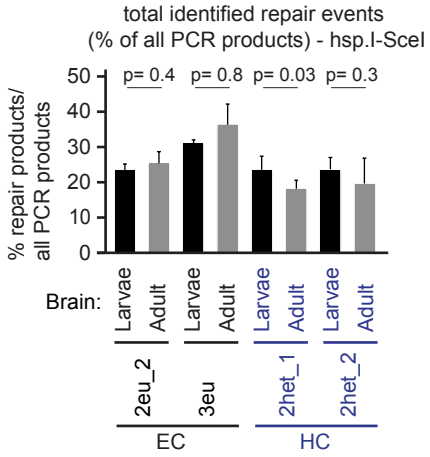


**Supplemental figure 5 (related to figure 5)**
Quantification of the percentage of TIDE-identified repair products from the total pool of PCR products in the larval (black bars) or adult brains (grey bars) with indicated DR-*white* insertions.

**Janssen, Supplemental Table S1**

| | | | | | attB construct | | | |
|---|---|---|---|---|---|---|---|---|
| **Annotation used in paper** | **Chromatin region** | **Integration site - release 6.0 coordinates** | **MiMIC line** | **Bloomington #** | **DRwhite** | ***i*white_SNP** | **LacO.I-Sce** | **TetO** |
| 2eu_1 | Euchromatin | described in Do et al., G3 2014 | x | x | YES | x | x | x |
| 2eu_2 | Euchromatin | 2R (51C1) - 14737964 | MI00794 | 32703 | YES | YES | YES | YES |
| 3eu | Euchromatin | 3L (61C7) - 626646 | MI03854 | 36965 | YES | YES | YES | YES |
| 2het_1 | Heterochromatin | 2L (40F6) - 22245311 | MI00127 | 30628 | YES | x | x | x |
| 2het_2 | Heterochromatin | 2R (h43) - 4013749 | MI00257 | 30681 | YES | YES | x | x |
| 3het_1 | Heterochromatin | 3L (80C4) - 23047118 | MI03233 | 36419 | YES | YES | YES | YES |
| 3het_2 | Heterochromatin | 3L (80E3) - 23284297 | MI02830 | 35885 | YES | x | x | x |
| 3het_3 | Heterochromatin | 3L (h52) - 27081070 | MI00192 | 30946 | YES | x | x | x |
| Xhet | Heterochromatin | X (20F4) - 23069456 | MI02024 | 32815 | YES | x | x | x |

| **Genotyping primers MiMIC sites*** | **Forward primer (5' of MiMIC insertion)** | **Reverse primer (3' of MiMIC insertion)** |
|---|---|---|
| 2eu_2 | GTCAAGGCACAGAAGGATAG | GATTGGGTTTAAATCAGAG |
| 3eu | GTCGTATTACTGCTGACGAC | GTGTGCGTGTGTGAGCCATG |
| Xhet | GATCCAAATAACCAGGCAC | CGATTTACACCTGCGAACG |
| 2het_1 | GTCGCTGTACAATTATTCAGC | CATTACTTATCGAGCGTC |
| 2het_2 | GAGCTAGATATGTACCAG | GATCTCGAGTTCATACGGAC |
| 3het_1 | GATCACGGCCATGCTTGACAAC | CCCACTTCGAAGACTCTA |
| 3het_2 | CCATAAAGTGTTCAGC | CTCCTTATGCGATTAAGCC |
| 3het_3 | GCAGATGTTGATGACCCCTTAC | GATCTGAGGTATAGCAAG |

| **Genotyping primers (constructs + controls)*** | **Forward primer** | **Reverse primer** |
|---|---|---|
| DRwhite_3xp3_iwhite | CTAATATCCTGCGCCAGCTC (downstream in construct) | CAGCTTACGCTTCGCGATG (upstream in construct) |
| 3xp3_iwhite_SNP | CAGTTCGGGCAAGGTCATCC (downstream in construct) | GCGACGTGTTCACTTTGCTT (upstream in construct) |
| LacO[256x]_3xp3_I-Sce[cut-site] | GTCTTCCGAGCTGTTTGAG (downstream in construct) | CAGACTAGTTCTAGAGTC (upstream in construct) |
| TetO[256x]_3xp3 | CCATGCGAAGCTCTCTAGG (downstream in construct) | GTAGGCCATCACTGGTCC (upstream in construct) |
| 3xp3 (internal control) | CTCGCCCGGGGATCTAATTC | GCGACGTGTTCACTTTGCTT |
| Actin (positive control) | GTGTGACGAAGAAGTTGCTG | GAGTCCAGAACGATACCGGTG |

| **qPCR/RT-PCR** | **Forward primer** | **Reverse primer** |
|---|---|---|
| yellow_qPCR | ACGGTCCACAGAAGAGGATT | GCACTTAGCTCTAAGCTGACA |
| I-Sce[cut-site]_qPCR | GAGCTGTAGGGATAACAGGG | CCGCCGGATTGTAGTTGGTA |
| rp49_qPCR | CTGTTTGTGATGGGAATTCG | CACAAGGTGTCCCACTAATG |
| Actinin_RT-PCR | TTGGAGGCGAGCGAATAA | TGGTCGCAGTTGTCCATC |
| CtIP_RT-PCR | GAACTTGAAGCAAACTCGCC | CTTGACTGTGCTATTGCTG |

| **Mutagenesis primers** | **Forward primer** | **Reverse primer** |
|---|---|---|
| iwhite_5'_SNP_mutagenesis | CATCAGCCGTCTTCAGAGCTGTTTGAGC | GCTCAAACAGCTCTGAAGACGGCTGATG |
| iwhite_3'_SNP_mutagenesis | GCTCTTTGACAAGATACTTCTGATGGCCGAGGG | CCCTCGGCCATCAGAAGTATCTTGTCAAAGAGC |

| **DRwhite PCR + sequencing** | **Forward primer** | **Reverse primer** |
|---|---|---|
| DRwhite_y+_2R1 amplification (for 2eu_1) | GTGGATCAGGTGATCCAGG | CTTAAGCCATCGTCAGTTGC |
| DRwhite_3xp3 amplification (for all but 2eu_1) | GTGCTGTGCCAAAACTCCTCTC | CGCGAATTCGTCGACATAAC |
| DRwhite_Sanger_seq primer | GAGCCCACCTCCGGACTGGAC | x |
| DRwhite_3xp3 constructs_SSA | CGTCGACGGAGCGTCAATTC | CCATCATGATGGTCGACAAGC |

* AttB constructs can be integrated in the two attP sites in two different orientations. Primer sets have been tested in different combinations to determine the orientation of the DR-*white*/*iwhite*/LacO and TetO integrations.

Cloning strategies:

DR-*white*

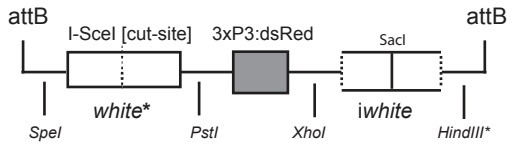


i*white* was first cloned into pBS.KSattB12 between the XhoI and HindIII site. Subsequently the *white*[I-SceI-cut-site] gene was cloned between SpeI and PstI. 3xp3.dsRed was cloned between PstI and XhoI. *HindIII site is not unique in final construct.

i*white*_SNP

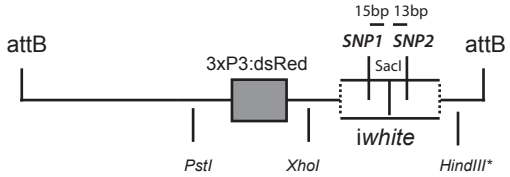


i*white_SNP* was first cloned into pBS.KSattB12 between XhoI and HindIII sites. 3xp3.dsRed was cloned between the PstI and XhoI sites. *HindIII site is not unique in final construct.

LacO[256x].I-SceI-cut site

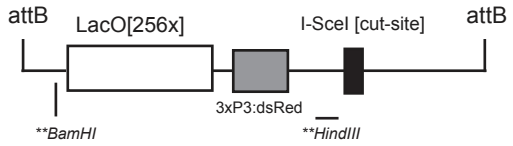


LacO[256x] was first cloned between the BamHI and HindIII sites.
Secondly, the I-SceI [cut-site] was cloned in the HindIII site using Infusion HD cloning kit (Clontech), leaving the upstream HindIII site intact.
Thirdly, 3xp3-dsRed was cloned in the HindIII site using Infusion HD, **which caused the HindIII site to be lost and the BamHI to not be unique in final construct.

TetO[256x]

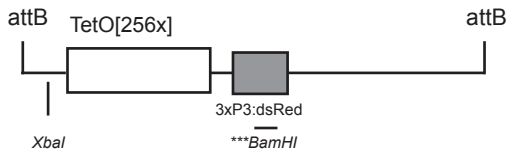


TetO[256x] cloned between the XbaI and BamHI sites.
3xp3-dsRed was cloned in the BamHI site using InFusion HD, causing ***BamHI to be lost.

**Supplemental Materials & Methods**
Cloning strategies for producing the DR-white, iwhite_SNP, TetO and LacO constructs in the pBS.KS.attB12 vector for integration in the MiMIC system.

**Janssen et al., Supplemental text Materials and Methods**

**Constructs**

DR-*white*, i*white*_SNP, LacO[256x].I-Sce$_{cut\text{-}site}$ and TetO[256x] constructs were cloned between 2 attB sites present in the pBS.KS.attB12 vector for targeted integration to specific MiMIC sites (Venken et al. 2011). The LacO 256x repeat sequence was cloned from pLacOp, a kind gift from Dr. Patrick Heun. The TetO 256x repeat sequence was cloned from a TetO containing plasmid, a kind gift from Dr. David Spector. All cloning steps for the LacO and TetO constructs were performed in Stbl2 bacteria (Invitrogen) to prevent recombination between repeats. The In-fusion HD cloning kit (Clontech) was used for cloning the LacO[256x].I-Sce$_{cut\text{-}site}$ and TetO[256x] constructs when restriction sites were limiting (Supplemental figure 1 Materials & methods). For creating the i*white*_SNP plasmids, two silent SNPs were introduced in an *iwhite*-containing pBS.KS.attB12 plasmid using the Quickchange mutagenesis kit (Agilent). Mutagenesis primers are listed in Table S1. For a schematic overview of the pBS.KS.attB12 plasmids cloned, and restriction sites used, see Supplemental figure 1 Materials and Methods.

eYFP-mu2 and ecDHFR-HA-I-Sce were each cloned upstream of a poly A sequence in a pCasper5 vector for random p-element transformation. The mu2 endogenous promoter was PCR amplified from genomic fly DNA and the mu2 coding sequence was PCR amplified from a mu2.GFP cDNA containing plasmid, a kind gift from Dr. James Mason. For creating the ecDHFR.HA.I-SceI plasmid, the ubiquitin promoter was PCR amplified from genomic fly DNA. The HA.I-SceI coding sequence was PCR amplified from a pUASt.HA.I-SceI plasmid and the ecDHFR clone #10 coding

sequence was PCR amplified from pBMN.ecDHFR#10.YFP, a kind gift from Dr. Tom Wandless.

**Sanger and Illumina Sequencing analysis**

The upstream *white* gene in the DR-*white* construct was amplified using a forward and reverse primer specific for the DR-*white* construct of interest (Table S1) with Herculase polymerase (Agilent) for 30 cycles.

For Sanger sequencing, PCR products were treated with 0.5µl ExoSAP-IT (Affymetrix) and subsequently sequenced by Genewiz with a DR-*white* Sanger sequencing primer (Table S1). Analysis of Sanger sequences was performed using the TIDE algorithm, a computational protocol designed by the lab of Dr. Bas van Steensel and previously published (Brinkman et al. 2014), available at http://tide.nki.nl. HR products were identified as conversions of the I-SceI recognition site to the wildtype *white* sequence (essentially a 23 basepair deletion). Insertions and deletions of up to 25 basepairs were categorized as indels (NHEJ products), with the exception of 23bp deletion products, which were categorized as HR products.

For Illumina sequencing, PCR products (100µl volume) were sonicated for 10 cycles on Bioruptor (Diagenode, high setting, 30'' on/off). Samples were treated with NEB next end prep (NEB). Illumina library preparation was performed using standard Illumina protocols and adapters. Illumina sequencing (100bp single reads) was performed on a Hiseq2500 by the QB3 Vincent J. Coates Genomics Sequencing Laboratory, UC Berkeley. Detailed analysis of HR and NHEJ products was performed

by a computational protocol designed by the lab of Dr. Bindra and previously published (Soong et al. 2015). Illumina sequence analysis for detecting the presence and abundance of SNPs in our DR-*white*_i*white*_SNP experiments (Fig.5) was performed using Bowtie2 alignment with the DR-*white* sequence as a reference genome.

**EdU labeling**

3rd instar larval wing discs were dissected and immediately incubated in 20µl PBS containing 10µM EdU for 30 minutes. Tissues were subsequently fixed for 10 minutes with 4% FA. EdU visualization was performed according to the Click-iT EdU Alexa Fluor 488 Thermo Fisher protocol (C10337). Immunofluorescence staining was performed on the same slides by overnight incubation with anti-phospho-S10 Histone H3 and anti- Cyclin A antibodies according to our standard IF protocol (see below).

**IF, FISH and FISH-IF**

For IF, tissues were blocked using PBS 0.4% Triton and 5% dried milk for 1 hour at room temperature. Primary antibody incubations were performed overnight at 4°C in a humidified chamber in PBS 0.4% Triton 5% milk. Slides were washed 3 times for 15 minutes each with PBS 0.4% Triton 5% milk. Secondary antibody incubations were performed at room temperature in PBS 0.4% Triton for 2 hours. Slides were subsequently washed 3 times for 20 minutes with PBS 0.4% Triton, incubated with

3µg/µl DAPI for 20 minutes, washed with PBS for 5 minutes and mounted using Prolong Antifade and a 22x22 mm no 1.5 coverslip (VWR).

For FISH staining, dehydrated tissues were washed 3 times for 5 minutes each with PBS 0.4% Triton and subsequently washed for 20 minutes in PBS 1% Triton, 0.1M HCl. Slides were then washed twice for 10 minutes in 2x SSC-T, 10 minutes in 25% formamide in 2x SSC-T and 10 minutes 50% formamide in 2x SSC-T. Slides were denatured in 50% formamide, 2x SSC-T for 1 hour at 37°C, 5 minutes at 50°C and 40 minutes at 70°C. 200ng probe in 12µl hybridization buffer (50% formamide, 10% Dextran Sulfate, 2x SSC-T) was denatured by heating at 95°C for 4 minutes, then immediately placed on ice for 4 minutes. Denatured probe was added to the slide (12 µl/slide), covered with a 22x22 coverslip, sealed with rubber cement and incubated overnight at 37°C in a humidified chamber. The next day, post-hybridization washes were performed: 30 minutes 50% formamide in 2x SSC-T (preheated) at 37°C, 60 minutes in 50% formamide, 2x SSC-T (at 37°C) and 10 minutes 25% formamide/2x SSC-T at room temperature. Finally, slides were washed three times for 5-10 minutes in 2x SSC-T and incubated with DAPI and mounted as described above for IF.

For IF-FISH, the IF protocol was performed as described above, except that the primary antibody incubation was performed at room temperature for 2 hours and the secondary antibody incubation was performed for 1 hour at room temperature. Slides were subsequently washed 3 times for 10 minutes in PBS 0.1 % Triton and post-fixed for 10 minutes with 4% formaldehyde. Following post-fixation, the FISH protocol was performed exactly as described above.

**Preparation of FISH probes**

For AACAC FISH, custom-made LNA probes coupled to Cy5 were manufactured by IDT Technologies. LacO, TetO and DR-*white* FISH probes were made using a random priming kit (Invitrogen, cat 18187-013) in the presence of aminoallyl-dUTP and pBSKS.attB12.LacO, TetO and DR-*white* containing plasmids as templates. Alexa dyes (Molecular probes, A32750, A32765 or A32757) were conjugated to aa-dUTP DNA fragments: Randomly amplified DNA was denatured in 10µl volume at 95°C for three minutes, placed on ice for 3 minutes and centrifuged at 3000 rcf for 3 minutes. 6µl 1M sodium bicarbonate was added to the DNA. 4µl DMSO was added to a single use Alexa-dye vial and vortexed. DNA and dye were subsequently mixed and vortexed for 15 seconds. The tubes with DNA-dye mix were incubated in the dark for 2 hours and vortexed twice midway. MinElute PCR purification kit (Qiagen) column was used to remove unincorporated dyes. The probe was precipitated overnight by adding 1/10 volume of 3M sodium acetate (pH 5.2) and 2.5 volumes 100% ethanol, spun at 11000 rcf for 15 minutes at 4°C and subsequently washed (2x) with 70% ethanol and centrifuging for 5 minutes at 11000 rcf. Probes were dissolved in FISH hybridization buffer (see above) for long-term storage at -20°C.

**References**

Brinkman EK, Chen T, Amendola M, van Steensel B. 2014. Easy quantitative assessment of genome editing by sequence trace decomposition. *Nucleic Acids Res* **42**: e168.

Soong CP, Breuer GA, Hannon RA, Kim SD, Salem AF, Wang G, Yu R, Carriero NJ, Bjornson R, Sundaram RK et al. 2015. Development of a novel method to create double-strand break repair fingerprints using next-generation sequencing. *DNA Repair (Amst)* **26**: 44-53.